ESTCP
Cost and Performance Report

(UX-9918)

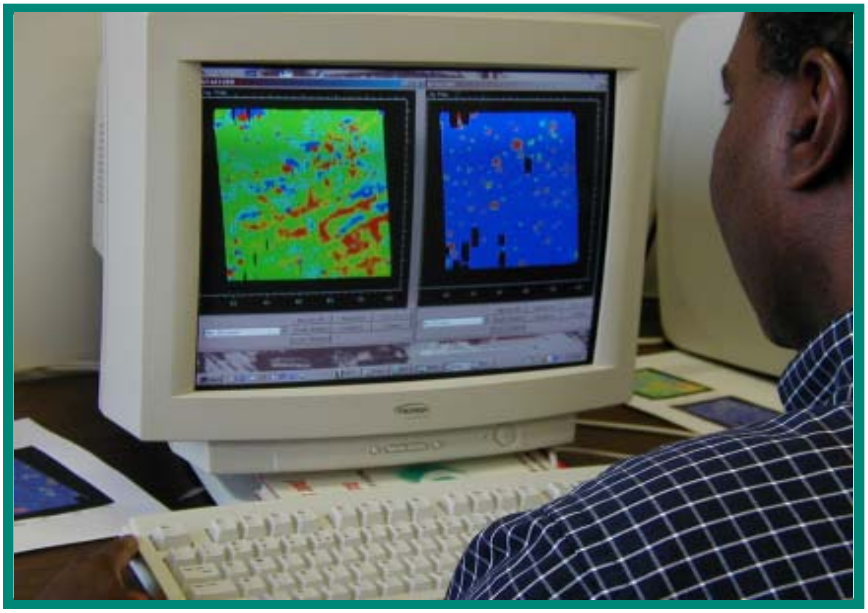

Matched Filter Processor for Detection and Discrimination of Unexploded Ordnance

August 2003

ENVIRONMENTAL SECURITY
TECHNOLOGY CERTIFICATION PROGRAM

U.S. Department of Defense

Report Documentation Page

Form Approved
OMB No. 0704-0188

1. REPORT DATE	2. REPORT TYPE	3. DATES COVERED
AUG 2003		**00-00-2003 to 00-00-2003**

4. TITLE AND SUBTITLE	5a. CONTRACT NUMBER
Matched Filter Processor for Detection and Discrimination of Unexploded Ordnance	5b. GRANT NUMBER
	5c. PROGRAM ELEMENT NUMBER
6. AUTHOR(S)	5d. PROJECT NUMBER
	5e. TASK NUMBER
	5f. WORK UNIT NUMBER
7. PERFORMING ORGANIZATION NAME(S) AND ADDRESS(ES) **Environmental Security Technology Certification Program (ESTCP),4800 Mark Center Drive, Suite 17D08,Alexandria,VA,22350-3605**	8. PERFORMING ORGANIZATION REPORT NUMBER
9. SPONSORING/MONITORING AGENCY NAME(S) AND ADDRESS(ES)	10. SPONSOR/MONITOR'S ACRONYM(S)
	11. SPONSOR/MONITOR'S REPORT NUMBER(S)

12. DISTRIBUTION/AVAILABILITY STATEMENT
Approved for public release; distribution unlimited

13. SUPPLEMENTARY NOTES

14. ABSTRACT

15. SUBJECT TERMS

16. SECURITY CLASSIFICATION OF:			17. LIMITATION OF ABSTRACT	18. NUMBER OF PAGES	19a. NAME OF RESPONSIBLE PERSON
a. REPORT **unclassified**	b. ABSTRACT **unclassified**	c. THIS PAGE **unclassified**	**Same as Report (SAR)**	**53**	

COST & PERFORMANCE REPORT
ESTCP Project: UXO-199918

TABLE OF CONTENTS

LIST OF FIGURES

LIST OF TABLES

LIST OF ACRONYMS

CDF	cumulative distribution function
DAS	Data Analysis System
EMI	electromagnetic induction
EOD	Explosive Ordnance Disposal
ESTCP	Environmental Security Technology Certification Program
JPG	Jefferson Proving Ground
JPG TD	Jefferson Proving Ground in Madison, Indiana, during the 2000 Advanced UXO Detection/Discrimination Technology Demonstration
MFAP	Matched Filter AutoProcess
MTADS	Multisensor Towed Array Detection System
ROC	Receiver Operating Characteristic
UXO	unexploded ordnance

ACKNOWLEDGMENTS

This work was supported by the Environmental Security Technology Certification Program (ESTCP) under contract DACA31-99-C-0075. The government liaison was George Robitaille. The data used for the demonstration of the Matched Filter AutoProcessor was collected by the Naval Research Laboratory with ESTCP sponsorship.

Technical material contained in this report has been approved for public release.

1.0 EXECUTIVE SUMMARY

1.1 BACKGROUND

The detection of Buried Unexploded Ordnance (UXO) is one of the most serious environmental problems facing the Department of Defense. In addition, false alarms due to clutter are also a serious problem. With traditional survey methods, the Army Corps of Engineers finds that 85-95% of all detected targets are not UXO. Since the cost of identifying and disposing of UXO in the United States using current technologies is estimated to range up to $500 billion, increases in performance efficiency due to reduced false alarm rates can result in substantial cost savings.[1,2] The investments of SERDP, ESTCP and the U.S. Army Environmental Center UXO Advanced Technology Demonstration Programs in automated UXO detection and discrimination technologies have resulted in site characterization technologies that have demonstrated detection probabilities of greater than 95 percent.[3] However, there are always buried targets that are too small, or are buried too deeply, to be detected with current systems. The Jefferson Proving Ground (JPG) Phase I-III demonstrations indicate improved system performance, but not necessarily an improvement in the size-depth detection envelope.[3,4,5] These detection results reflect the performance of experienced operators selecting anomalies from displays of survey data. Studies of visual signal detection consistently show that human operators do not perform as well as the optimal linear processor. Human observer efficiency for detection of aperiodic signals in white noise is about 50% and is further reduced with the addition of structured noise.[6] Reported detection efficiencies in structured backgrounds are 10% for detection of disk signals in simulated lumpy backgrounds consisting of Gaussian-shaped blobs,[7] 4% to 17% for detection of simulated lesions in backgrounds representative of coronary angiograms,[8] and 36% for detection of a vehicle in natural settings.[9] However, optimal linear filtering has not been used previously for UXO detection. Such a processor is based on thresholding the output of a prewhitening matched filter[10] that compensates for any background correlation structure (prewhitens) and then correlates the data with the expected signal. It is optimal in that it maximizes the output signal to noise ratio, and is variously referred to in the pattern recognition and medical imaging literature as the Fisher linear discriminant, the Hotelling observer or the Fisher-Hotelling model. If the noise statistics are Gaussian, it corresponds to the maximum likelihood detector and maximizes probability of detection.[11]

In this project, we have developed a Matched Filter AutoProcessor (MFAP) that implements an optimal linear filter in a threshold-based UXO detection processor. It also implements screening procedures based on target attributes (e.g., size, depth, orientation) determined from their magnetic signatures, in order to discriminate between UXO and the false alarms due to metallic clutter. The individual screening criteria compare the various target attribute values with threshold levels set by the user. The results of the individual tests are combined using Boolean logic, allowing the user to specify which attributes to include in the logical sum. It is expected that the MFAP will provide improved detection performance for weak/deep targets in magnetically active or noisy areas. The detection and classification modules can be added to existing detection and analysis systems. In addition to improving detection of targets in magnetically noisy areas, the matched filter also reduces ambiguity in the location of a target, because the filter output peaks directly over the target location (unlike raw magnetometer data, for which the center of the dipole pattern is not typically at the target location).

The Matched Filter AutoProcessor was developed and tested using the Interactive Data Language (IDL). This report discusses details of the algorithm and presents performance measures. Upon successful completion and acceptance of the development effort, the codes were rewritten in C++ language to create a dynamic link library that interfaces with the OASIS Montaj processing environment. OASIS Montaj is developed and marketed commercially by Geosoft, Inc. Appendix B presents a discussion of OASIS Montaj integration effort. The Matched Filter software (matchfilter.gx and matchfilter.dll) and documentation (Matched Filter ReadMe.doc) are available for download via the ESTCP website.

1.2 OBJECTIVES OF THE DEMONSTRATION

The objective of the demonstration was to show whether the MFAP improves UXO detection and false alarm rejection relative to procedures currently used in the field, particularly for weak/deep targets in magnetically active or noisy areas. The demonstration of this automatic processor was performed on magnetometer data collected during the more recent 2000 UXO Detection/Discrimination Advanced Technology Demonstration at the Jefferson Proving Ground in Madison, Indiana (henceforth called JPG Technology Demonstration, or JPG TD). This demonstration took place on three 1-hectare sites that contained both inert UXO and typical ordnance scrap specifically seeded into a magnetically active geological environment. The JPG TD demonstrators (who all used active EM systems) were asked to detect, locate and identify UXO in the three areas, producing a target list with recommendations for each target whether the item should be dug or could confidently be left in the ground.[12] The demonstration of this matched filter autoprocessor used magnetometer array data collected over the same sites and followed the same requirements, to the extent that the magnetometer (rather than electromagnetic) data and this technology allow. The ground truth of the JPG Technology Demonstration was used to determine the performance of the matched filter processor.

1.3 DEMONSTRATION RESULTS

The curves below are the Receiver Operating Characteristics (ROCs) for the primary demonstrators at JPG TD, who used electromagnetic induction (EMI) systems. The three colored points on each plot indicate the relative performance of analysis of magnetometer data using the MFAP and U-Hunter, as well as standard Mag and Flag methodology. U-Hunter and Mag and Flag points generally lie far to the right of the curves, indicating significantly poorer performance. The MFAP points, on the other hand, reveal performance comparable to the best demonstrators in Area 2, and intermediate between the various demonstrators in Areas 1 and 3.

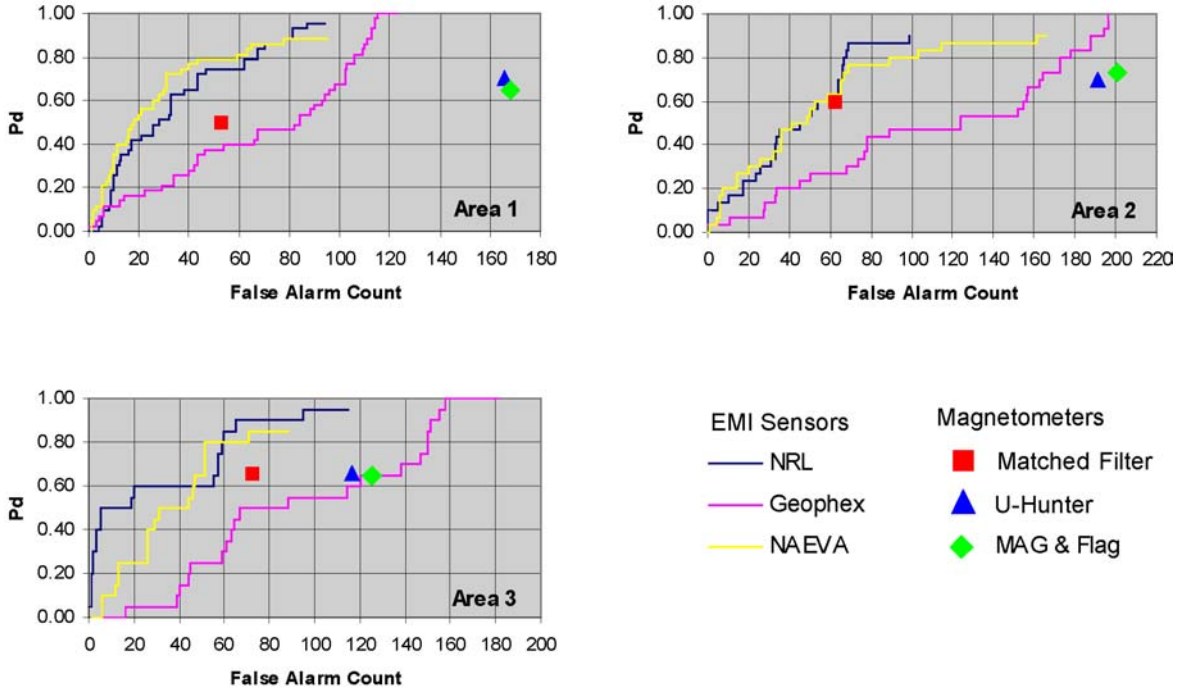

2.0 TECHNOLOGY DESCRIPTION

2.1 TECHNOLOGY DEVELOPMENT AND APPLICATION

Buried Unexploded Ordnance (UXO) is one of the most serious and prevalent environmental problems currently facing Department of Defense facility managers. SERDP, ESTCP and the U.S. Army Environmental Center UXO Advanced Technology Demonstration Programs have been addressing the need for automated UXO detection and discrimination technologies for several years. These investments have resulted in technologies that have demonstrated UXO detection probabilities of greater than 95 percent.[3] The detection results reflect the performance of experienced operators selecting anomalies from displays of survey data. Studies of visual signal detection, notably in the medical imaging community, consistently show that human operators do not perform as well as the optimal linear processor.[6,7,8,9] The optimum linear detection processor maximizes the output signal to noise ratio, and if the noise statistics are Gaussian, it corresponds to the maximum likelihood detector and maximizes probability of detection.[11]

In addition to detection of UXO, false alarms due to clutter (signals incorrectly diagnosed as having been caused by UXO) remain a serious problem. The Army Corps of Engineers finds that 85-95% of all targets detected with traditional survey methods are not UXO. Since the cost of identifying and disposing of UXO in the United States using current technologies is estimated to range up to $500 billion, increases in performance efficiency due to reduced false alarm rates can result in substantial cost savings.[1,2]

The Matched Filter AutoProcessor (MFAP) we have developed is an optimum linear detection processor. It is expected that this processor will provide improved detection performance for weak or deep targets in magnetically active or noisy areas. The MFAP also applies Boolean logic to target attribute screening, in order to rationalize the UXO/clutter discrimination process and reduce false alarms. The signatures of clutter items that cause false alarms can be subtly different from the signatures of UXO items, and experienced operators do some screening of the field anomalies to eliminate obvious false alarms. Anomaly characterization procedures in the Data Analysis System developed by AETC for use with MTADS estimate, for each detected object, various target attributes from the measured magnetic anomaly. Systematic and objective target screening criteria for the MFAP are based on these attributes.

The detection and classification modules can be incorporated into the existing Multisensor Towed Array Detection System (*MTADS*) Data Analysis System developed by NRL, or other systems, and serve in the future as a testbed for exploring site-specific optimization of threshold settings and decision rules for UXO detection and false alarm rejection. The processor's target selection routine should provide more automatic and thus efficient target selection and thus lower expenses for large survey areas. In addition, future versions of the MFAP can be modified to analyze active electromagnetic system data as well as passive magnetometer data.

2.2 PROCESS DESCRIPTION

In general, a matched filter operates by convolving the data with an appropriate signal model, accompanied by a search over the unknown parameters in the signal model to maximize the filter output. Detections are called when the filter output exceeds some threshold. This threshold can be varied to achieve the desired performance. The MFAP operates on magnetic survey data and uses a filter based on a magnetic dipole at a given depth. It maximizes the filter output at each assumed target horizontal location with a search over size and orientation of the magnetic moment. The matched filter output is enhanced at locations where the data fits the model well. In other words, UXO whose depths are close to the chosen filter depth will show up in the filtered data as peaks standing out above the background. The filter output near objects that are not dipole-like (e.g., geologic features that may have strong signatures in the raw data) or are not compact (e.g., magnetic soil) will be suppressed.

Since the depths of the expected targets are unknown, the filtering procedure is repeated over several filter depths. We have observed that deep targets ring out strongly over a relatively wide range of filter depths, so the filter depths can be spaced at half-meter or even one-meter intervals. For each filtered depth, the image created from the matched filter output is contoured and peaks are identified as provisional (dipole-like) targets. Multiple targets at the same location selected from several depths are reduced to a single provisional target. The horizontal location of each provisional target is then input to a dipole-fitting routine whose outputs include fitted dipole depth, size, orientation, and coherence (a goodness of fit parameter).

Since some objects that are not UXO (e.g., metallic clutter or magnetic rocks) can also give compact dipole signals and be identified as provisional targets, we have implemented screening procedures based on the target attributes determined from their magnetic signatures, in order to reduce false alarms. The individual screening criteria are based on comparison of the target attribute values with threshold levels set by the user. The results of the individual tests are combined using Boolean logic, allowing the user to specify which attributes to include in the logical sum.

The four processing steps are summarized below. More detail on the processing can be found in the project final report.[13]

Step 1: Filter the magnetic data

- the magnetometer data is mapped and interpolated to a regular x-y grid
- the operator selects a set of target depths for the matched filter, based upon the expected types of ordnance and their maximum depths
- for each depth, the matched filter runs automatically on the data, also removing any local linear magnetic background in the data as it filters

The choice of the filter depth is not critical. The filter creates a filter box around each data point in the image to perform the dipole fit and background subtraction on the data. The size of the filter box increases with increasing filter depth, in order to capture the increasing width of a dipole's signature at the sensor. As currently implemented, the algorithm cannot filter a data

point if there are any missing data in the filter box. Thus, the edges of a survey site (half a filter box width) cannot be filtered, as well as any interior regions that are missing raw data (e.g., because of poor navigation or obstacles in the survey field). For a filter depth of 0.5 m, a (typical) strip of missing magnetometer data 0.5 x 5 m (2.5 m^2) becomes an unfilterable region 5.4 x 9.9 m (52.9 m^2). For larger filter depths, this problem becomes more severe. However, the increased area lost at deeper depths overstates the number of potential targets lost. Because the majority of deep targets also show up in images filtered at shallower depths, a deep target that lies in a data gap at a large filter depth may lie outside that gap at a shallower depth.

Step 2: Identify peaks in the matched filter output as provisional targets

- for each target depth chosen, the filter output is displayed as an image
- the operator selects a detection threshold and an automatic peak-selector detects threshold exceedances in the output field

The peaks in the filter output image are found with a contouring threshold procedure. The operator can use the default threshold value, derived from the cumulative distribution function (CDF) of the filter output, or select a different threshold if the default results show missed targets that are obvious strong dipoles, or if there are too many weak and possibly spurious targets selected. Our tests on vehicular *MTADS* magnetometer data from several sites showed that a threshold value equal to the filter output for a CDF of 0.75 performed satisfactorily. Filtered data is contoured with levels lying between the threshold and the maximum filtered data level. Maximum points within concentric contours are identified as peaks or provisional targets. After provisional targets are selected from each filter depth, duplicate targets (chosen at a location for more than one filter depth) are removed in order to get the final list of provisional targets.

Step 3: Fit provisional targets to magnetic dipole model

- the x-y location of each provisional target is input to a dipole fitting routine that estimates the best dipole fit from the data
- the targets are tabulated with the dipole-fitting output: fitted dipole depth, moment, radius, orientation and data/model coherence (a goodness-of-fit parameter that ranges from 0 to 1.0.)

Step 4: Screen and sort the provisional targets on the basis of expected target attributes, combining the individual screening results with Boolean logic

- targets are eliminated which do not fit a dipole model well
- targets are eliminated whose fitted sizes/depths are too large/small to be UXO
- any additional target attributes expected for the particular site or type of ordnance is used for screening
- the remaining targets are ordered by closeness of fitted dipole moment angle to the Earth's field
- the operator selects a dipole moment angle threshold to separate UXO from clutter

The *data/model coherence* is an important screening parameter. The dipole contribution dominates the magnetic signature of a UXO item at any sensible range. Some clutter items (e.g., buried sheet metal, sections of wire), on the other hand, are expected to exhibit significant departures from the dipole model and thus have a lower data/model coherence value. The threshold on coherence is selected by determining the coherence values that detect all obvious strong dipoles in the data without adding large numbers of clearly spurious targets. In general, we find a coherence threshold of 0.8 to be adequate. The MFAP removes objects from the provisional target list that (a) are too weak to determine their fit to a dipole model, and (b) fit a dipole model with coherence less than the selected threshold.

Our dipole-fitting procedures reliably estimate *target depth* to within less than 10%.[14] This can be used to eliminate objects that are deeper than the deepest UXO expected for the survey area. Much of the clutter is due to small metal fragments at or near the surface, and can often be rejected by screening on the basis of *target size*. Target size estimates are not as accurate as depth estimates, since for typical UXO the strength of the magnetic signal (and thus derived size) varies somewhat with the orientation of the target. Our experience with UXO of various sizes, buried at various depths and orientations, is that the size estimates have a standard deviation of about 30% around the actual ordnance caliber, which will usually suffice for distinguishing between shell fragments and intact UXO.[15] It will also suffice to screen out objects that are too large or small to be UXO of the types expected for the survey area.

Dipole orientation can also be a useful screening parameter. At least some clutter items have a different distribution of dipole orientations than that of UXO[16,17,18] Ordnance items tend to have low remnant magnetization due to their construction (cast as opposed to rolled or drawn) and/or history (the shock effects of firing and impact with the ground), so their dipole moments are due solely or mostly to the Earth's field. For all possible orientations of a demagnetized ordnance item there is a maximum possible angle θ_{max} between the induced dipole moment and the Earth's magnetic field; this angle is determined by the aspect ratio of the ordnance. Clutter items, on the other hand, can have significant remnant magnetic moments, resulting in a broader distribution of dipole orientations; their dipole moments can be found at all possible angles to the Earth's field. This difference in dipole moment orientation is used in the MFAP to reject as clutter all objects with moments oriented at angles to the Earth's field larger than θ_{max}. (Note that both measurement error and the types of UXO expected in the survey area need to be taken into account when θ_{max} is determined.) Among the objects with angles less than θ_{max} one expects to find all the ordnance, as well as some of the clutter.

Additional target attributes or correlations between attributes can also be used as screening criteria as they become recognized with more data analysis. For the demonstration on JPG TD data, as described in section 4.1, an additional screening criterion was added to two of the survey areas after the ground truth from the one of the areas was received and reviewed: the added criterion was the correlation between the data/model coherence and the fitted depth.

After screening of provisional targets is completed, the remaining targets can be ordered by closeness of the fitted dipole angle to the Earth's field.

3.0 DEMONSTRATION DESIGN

3.1 PERFORMANCE OBJECTIVES

The demonstration of the MFAP was not performed in the field; it was instead performed in contractor offices using magnetometer array data previously collected at Jefferson Proving Ground in Madison, Indiana, during the 2000 Advanced UXO Detection/Discrimination Technology Demonstration (JPG TD).[12]

The performance objectives of the matched filter autoprocessor are to improve detection and discrimination of UXO, particularly for weak or deep targets in magnetically active or noisy areas. The performance metrics are probability of target detection and probability of false alarms.

Table 1. Performance Criteria.

Performance Criteria	Description	Primary or Secondary
Hazardous Materials	Using magnetometer data, detect UXO in the size range from 20 mm to 155 mm projectiles. Determine the probability of detection.	*primary*
Reliability	Determine the percentage of false alarms.	*primary*
Ease of Use	Determine how much training is necessary to obtain optimal results.	*secondary*

3.2 SITE CHARACTERISTICS

This demonstration was performed in the Arlington, Virginia, offices of AETC, using data that was previously collected on a government range (JPG) for other purposes. There are thus no regulatory, health or safety issues affecting this demonstration. However, the details of the demonstration site, operations, and analysis requirements are relevant to this demonstration, since the results of the processor are compared to the results of the JPG demonstration.

The JPG demonstration prepared three 1-hectare sites containing inert UXO, ordnance scrap, and magnetic soils/rocks. Two of the three sites took advantage of naturally-occurring magnetic soil deposits. Three demonstrators were invited to participate using active electromagnetic sensors; the NRL man-portable EMMS, Geophex with a variant of the GEM sensor and NAEVA with the Geonics EM-63 sensor. Each demonstrator was asked to conduct digitally-mapped geo-referenced surveys and to conduct target analyses on site as though concurrent remediation would take place. Ten types of inert ordnance were included, varying in size from 20-mm aircraft-fired projectiles to 155-mm howitzer projectiles. Demonstrators were told that emplaced inert ordnance was degaussed. The non-UXO items were only described as realistic ordnance scrap.

The demonstrators were also asked to produce a list of detected targets prioritized as UXO or not-UXO with an associated degree of confidence, and a recommendation for which targets should be dug and which could confidently be left in the ground. Two independent analyses and lists were to be submitted, based upon whether or not 20-mm projectiles were assumed to be present. The onsite EM surveys and analysis products were to be evaluated on the basis of cost/production rates, UXO detection rates, target location accuracy and UXO identification ability.

The JPG demonstrators deployed and were evaluated on use of active electromagnetic sensors. In addition, an independent survey was made of the three sites using the NRL vehicular *MTADS* magnetometer array. These data were preprocessed to create geo-referenced mapped data files that were provided to each of the other demonstrators following their reporting of EM results, for optional joint magnetometer-EM data analyses. This *MTADS* magnetometer data set was analyzed by the MFAP. The target list produced by this analysis was prioritized into UXO and not-UXO with confidence categories, in a manner similar to the three JPG TD demonstrators.

4.0 PERFORMANCE ASSESSMENT

4.1 DEMONSTRATION DATA ANALYSIS

The primary performance criteria for the Matched Filter AutoProcessor (MFAP) are probability of detection and probability of false alarm. A secondary performance measure is the ease of using the MFAP in terms of operator training necessary to obtain satisfactory results. The data used to estimate these measures is vehicular *MTADS* magnetometer data from the JPG TD. The seeded UXO ranged in size from 20-mm aircraft-fired projectiles to 155-mm howitzer projectiles. The non-UXO items buried in the survey areas were realistic ordnance scrap, but were not described further. We were informed that all ordnance was demagnetized before burial. Target lists for the three JPG TD survey areas were produced. The detected targets were sorted into categories of UXO and not-UXO, with confidence levels associated with each target.

The vehicular *MTADS* sensor array was 0.25 m above the ground. In the standard pre-processing the data was gridded and mapped to 0.25 m spacing in both x and y. All depths for buried objects (dipole sources, UXO, clutter, etc.) are referenced to the surface of the ground, and are positive downward.

Step 1: Filter the magnetic JPG TD data

Figure 1 shows raw and filtered magnetometer images from JPG TD Area 2. The raw data (on the left) shows strong, extended geologic features. The second image shows the filter output for a filter depth of 0.10 meters. One can see that the filter does an excellent job of removing the strong, extended geologic features in the raw magnetometer data and producing isolated peaks in the filter output.

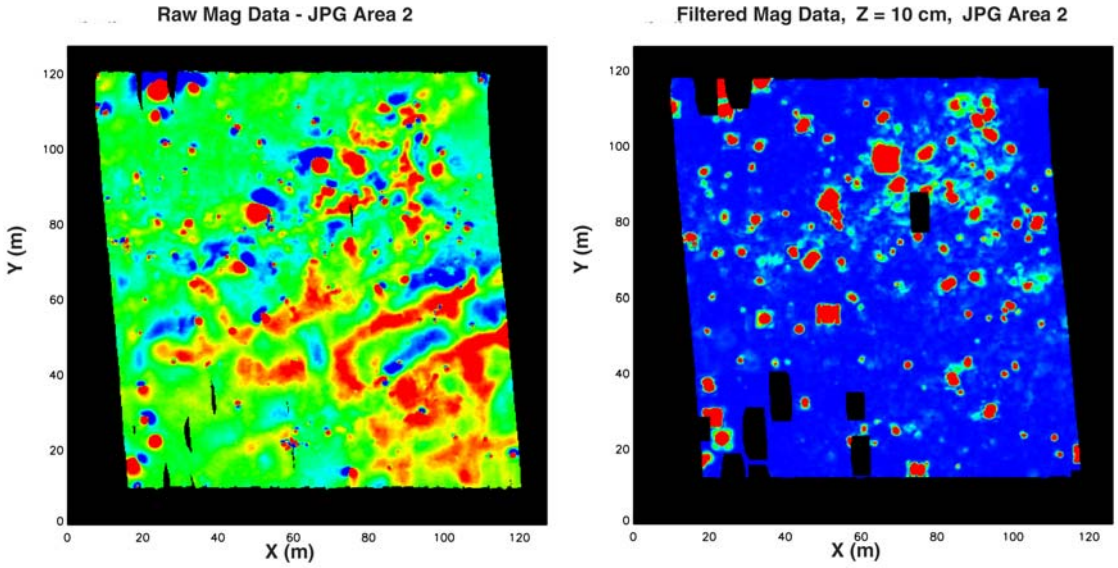

Figure 1. Raw and Filtered Magnetometer Data for JPG TD Area 2.

The choice of the filter depth is not critical. We have found that deep targets ring out strongly in the MFAP output over a relatively wide range of filter depths, as shown below in Figure 2 for JPG TD Area 3. The images show the data filtered at 0.1 meter (left) and 2.0 meters (right); deep targets are clearly visible at both the deep and shallow filter depths.

Thus, for the JPG TD data, the filtering procedure was performed with only 5 filter depths. A shallow filter depth (0.10 m) was used to identify the overwhelming majority of both the shallow and deep targets. Three deeper filter depths (1.0, 2.0, and 3.0 m) were used to identify additional deep targets that were not clearly visible in the 0.10 m filtered output. The last (0.50 m) filter depth was used to identify any targets that might lie between 0.10 and 1.0 m but were too small to appear unambiguously as targets in the 0.1 m images. (Note that when we performed spot checks by filtering the data at other depths, no additional targets were found.)

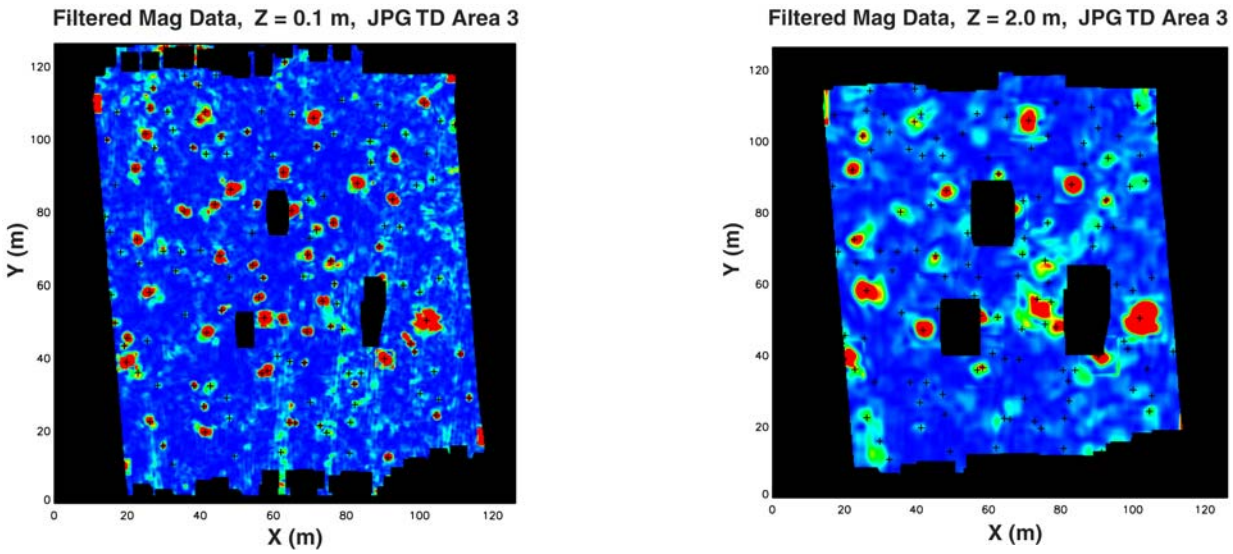

Figure 2. Target Locations (Crosses) from JPG TD Area 3 Overlaid on Filter Output Images at Shallow and Deep Filter Depths, 0.1 m (left) and 2.0 m (right).

Figures 1 and 2 show that the filtered images contain regions without any matched filter output. The MFAP creates a filter box around each data point in the image to perform the dipole fit and background subtraction on the data. The size of the filter box increases with increasing filter depth, in order to capture the increasing width of a dipole's signature at the sensor. As currently implemented, the algorithm cannot filter a data point if there are any missing data in the filter box. Thus, the edges of a survey site (half a filter box width) cannot be filtered, as well as any interior regions that are missing raw data (e.g., because of poor navigation or obstacles in the survey field). Figure 3 shows data from JPG TD Area 1 filtered at 0.1 m and 3.0 m depths. The area lost at the edges is 10% for the 0.1 m filter depth and 25% for the 3.0 m filter depth. The area lost to interior data gaps is 3% and 8%, respectively, for the two filter depths. However, the increased area lost at deeper depths overstates the number of potential targets lost. As discussed above, the majority of deep targets also show up in images filtered at shallower depths, so a deep target that lies in a data gap at a large filter depth may lie outside that gap at a shallower depth.

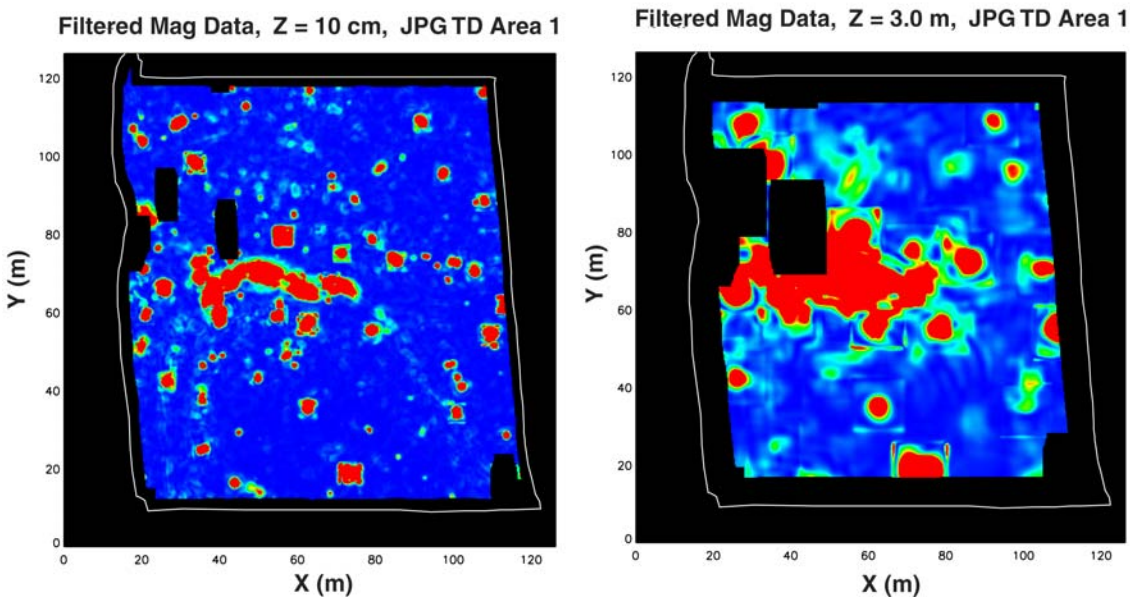

Figure 3. Data from JPG 2000, Area 1, Showing the Increase in Size of the Data Gaps with Filter Depth, from 0.1 m Filter Depth (left) to 3.0 m Filter Depth (right).

Step 2: Identify peaks in the matched filter output as provisional targets

When the default contour threshold for picking targets was determined from the global cumulative distribution function (CDF) of the filter output over each survey area, we found that a huge number of spurious peaks were picked over the entire region, especially around the stronger targets. The shape of the CDF over an entire JPG TD area was markedly different from that over a small sub-patch. The solution was to break each JPG area into smaller areas (30 m on a side) and perform independent contour thresholding based on the local CDF (using the usual 75% threshold). From this procedure, a reasonable number of provisional targets were identified by the autoprocessor.

Table 2 shows the number of provisional targets found in JPG TD Area 2 after filtering at the five depths and removing duplicate targets. The results for Areas 1 and 3 were similar.

Table 2. Provisional Targets from JPG TD Area 2.

Filter depth (meters)	Number of Targets Found	Percent of Total Targets
0.1	170	77
0.5	15	7
1.0	20	9
2.0	11	5
3.0	4	2
Total	**220**	**100**

Step 3: Fit provisional targets to magnetic dipole model

A number of peaks identified by the matched filter autoprocessor were too weak to fit to a dipole model. These were eliminated from the target list without further analysis.

Step 4: Screen and sort the provisional targets on the basis of expected target attributes

The original target screening attributes used were data/model coherence, fitted target size, fitted target depth. After determining a cutoff for each target attribute and screening the provisional targets, the remaining targets were ordered by closeness of the fitted dipole orientation to the Earth's field. Dig lists were produced from these criteria.

However, after the ground truth from JPG TD Area 3 was received, the results were analyzed to see if there should be any modifications in or additional screening criteria for the final target lists for Areas 1 and 2. There were two changes, discussed further below, made to the screening criteria: (1) the buffer zone in dipole orientation to the Earth's field was removed and (2) targets with joint deep fitted depths and relatively low model/data coherence were eliminated from the target list.

The data/model coherence cutoff was 0.8, as determined from our experience with data from other surveys. This removed a large number of provisional targets (30%-40%). Several targets with coherence less than 0.8 were nevertheless retained in the target list because there were obvious navigation errors in the data that produced the low coherence. (Note that some of the targets in Area 3 rejected for low coherence for non-navigation reasons did turn out to be ordnance, as discussed in the next section.)

Since, as previously discussed, size estimates derived from the dipole fitting routine have a standard deviation of about 30% around the actual ordnance caliber, we used a 45% (a 1.5 σ) rejection window. We rejected all provisional targets whose fitted size was smaller than 55% of the smallest expected UXO or larger than 145% of the largest expected UXO. For the JPG TD, these were 20 mm projectiles and 155 mm howitzers, respectively. The results of this screening rejected no targets because they were too small, and rejected only 1 (out of 674 provisional targets in all three areas) because it was too large.

Objects that were deeper than the deepest expected UXO were also screened. Only 1 target was rejected as too deep for the JPG data; the fitted depth for that object was greater than our threshold of 4 meters.

For the orientation-angle screening criterion, we calculated the maximum expected angle (θ_{max}) between the induced dipole moment of a non-magnetized object and the Earth's field. This angle θ_{max} increases with increasing aspect ratio. The ordnance in JPG TD with the largest ratio was the 2.75 in rocket (aspect ratio 6.5:1); the corresponding maximum allowed angle is 57°.

Figure 4 shows, for Areas 1, 2 and 3 (left to right), shaded in red, the possible azimuth-inclination combinations possible for a cylinder with a 6.5:1 aspect ratio with no remnant magnetization. The region has a sharp boundary, corresponding to the maximum allowed angle

θ_{max} of 57°. Superimposed on this plot are the dipole-fitting routine's azimuth and inclination fits for all the provisional targets in the three areas that had coherences above the cutoff of 0.80 (blue triangles). Those items within the red shaded region may be ordnance and therefore should be dug up; ordnance should not be found outside the red shaded region.

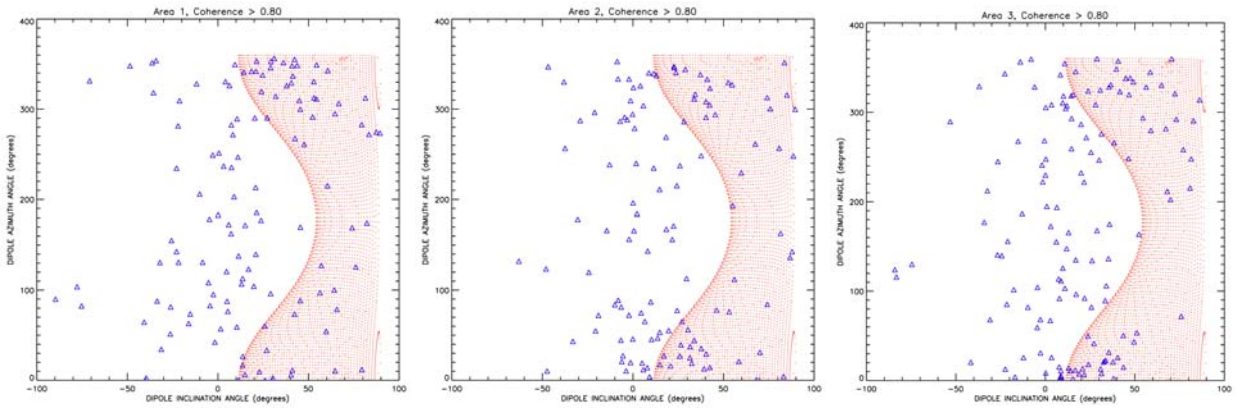

Figure 4. Possible Azimuth-Inclinations for a 6.5:1 Aspect Ratio Cylinder with No Remnant Magnetization, for Areas 1, 2, 3 (left to right). (The blue triangles are the provisional targets with coherences above 0.80.)

There are uncertainties in the dipole fitting routine's estimates of the induced dipole moments of the provisional targets and ordnance items may have some remnant magnetization. Thus, some ordnance items may lie outside the red region in Figure 4. To account for these inaccuracies, the initial decision was to add a buffer zone of 23° and set 80° as the cutoff cone angle between possibly ordnance and definitely clutter. The value of 80° is in agreement with the largest angles we have observed for ordnance at other sites. However, in reviewing the ground truth results for Area 3, we observed that all of the ordnance items fell within θ_{max}, and none fell in the buffer zone between 57° and 80°. We therefore decided that we were too conservative in our angle cutoff and we removed the buffer zone in the criteria for Areas 1 and 2. The results discussed in this report and the final dig lists for Areas 1 and 2 (which can be found in the final report[13]) are without the buffer zone in the angle criterion.

A final screening criterion was developed from reviewing the ground truth for JPG TD Area 3. Figure 5 shows, for all targets in Area 3 that passed all the screening criteria, their fitted depth and the data/model coherence. The targets that are truly ordnance are plotted as blue-filled diamonds. It is clear that there are no UXO with joint low coherences and deep fitted depths.

This is reasonable when it is considered that larger projectiles or bombs will likely bury themselves deeper in the ground than smaller ordnance, and for these larger objects the signal and data/model coherence is expected to be stronger than for clutter. Thus, objects with coherences below 0.93 and depths below 0.6 m were moved into the dig list category of high confidence clutter, regardless of their other target attribute values.

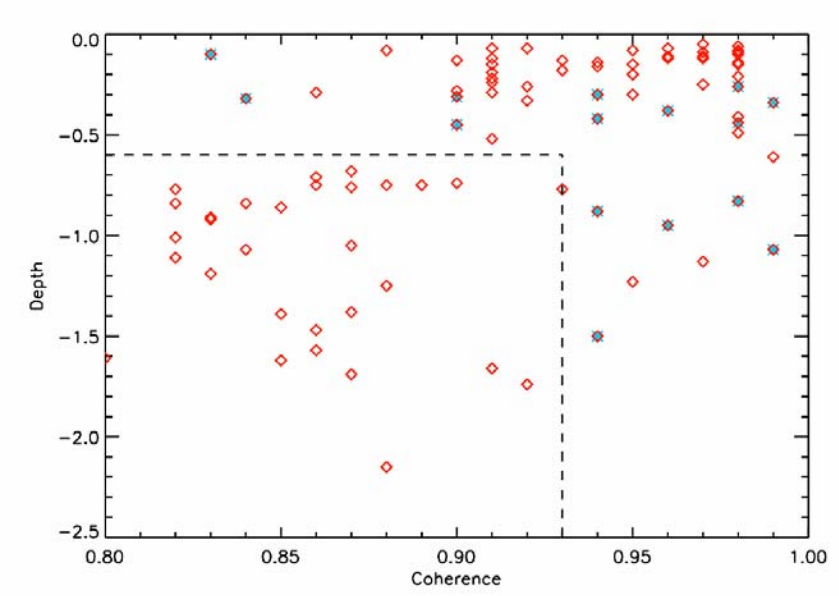

Figure 5. Fitted Depth and Data/Model Coherence for Targets Selected for JPG TD Area 3, after Screening, Plotted as Open Red Diamonds. [Targets that are truly ordnance (determined from ground truth) are blue-filled diamonds. The dotted line divides the target area from an excluded area.]

The targets that passed all the screening criteria above were then sorted by the closeness of the fitted dipole moment to the Earth's field, and all targets were given confidence levels on their categorization as ordnance or clutter. The objects in the final dig list above the "do not dig below" line are those that fit a dipole model well, that were not bigger, smaller or deeper than the expected UXO types, were not too deep for the coherence value, and whose dipole orientation could be induced by the Earth's field. However, if an object fits all these criteria, there is no objective measure to discriminate among them, and the final dig list therefore has only two categories: (1) high confidence clutter and (2) ordnance-or-clutter.

Table 3 shows the final screening results for JPG TD. For Area 3, these results are based on the original screening parameters. For Areas 1 and 2, the modified screening based on information from Area 3 ground truth were used.

Table 3. Final Target Screening Results for JPG TD.

Screening Criteria	Area 1	Area 2	Area 3
total # of targets before screening	**213**	**220**	**241**
rejected (too weak to fit as a dipole)	24	36	55
rejected (too small)	0	0	0
rejected (too large)	0	1	0
rejected (too deep)	0	1	0
rejected (data/model coherence < 0.8)	60	63	47
replaced in list (coh < 0.8 but nav errors)	6	0	0
Total # of targets after screening	**129**	**119**	**139**
ordnance or clutter ($\theta < \theta_{max}$)	50	53	91
clutter with high confidence ($\theta > \theta_{max}$)	79	66	48

Note that, after all non-UXO were eliminated because of the criteria on target attributes of size, depth, and data/model coherence, the remaining targets were ordered by closeness of fitted dipole moment direction to that of the Earth's field. Then the operator can classify the targets with moment angles outside the maximum expected angle as high confidence clutter and the targets with moment angles within the maximum expected angle can be classified as ordnance or clutter. However, the MFAP analysis of magnetometer (rather than electromagnetic) array data cannot discriminate further among these categories.

Figure 6 shows the final filter output images for Areas 1, 2, 3 for a filter depth of 0.1 m. The targets that were recommended to dig up are marked with crosses. For the image from Area 3, the seeded ordnance are marked with triangles (19 items) and the seeded clutter are marked with diamonds (34 items). It can be seen that there are some seeded clutter items that were selected to dig (10 items), and others that were not (24 items).

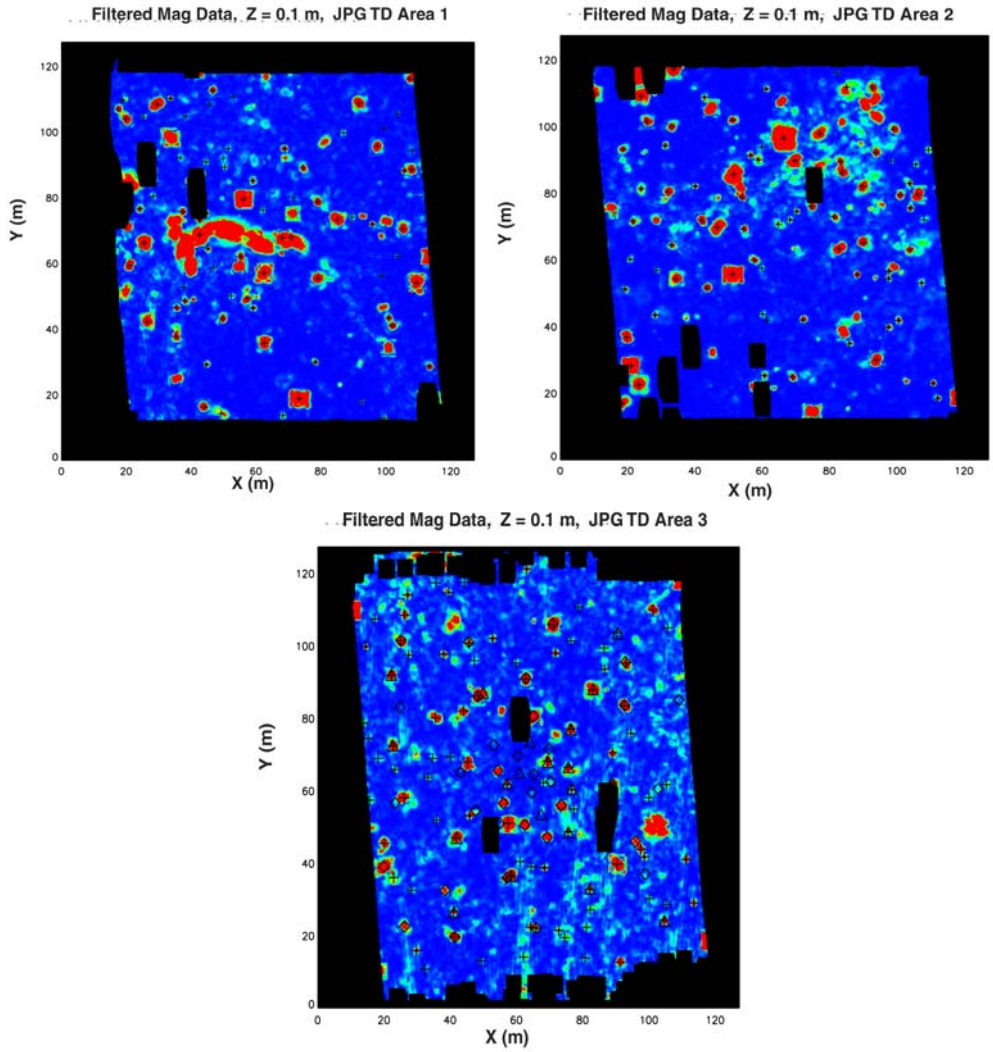

Figure 6. Filter Output Images for JPG TD Area 1 (left), 2 (right) and 3 (bottom) for a Filter Depth of 0.1 m. (Targets to dig up are marked with crosses. For Area 3, the seeded ordnance are marked with triangles; seeded clutter are marked with diamonds.)

4.2 PERFORMANCE

The matched filter autoprocessor (MFAP) appeared to do a good job of isolating potential targets in the magnetically noisy and active areas encountered in JPG TD. This was in agreement with the results of our previous tests using the filter on several other sites (Laguna, Buckley, Blossom Point, Twentynine Palms). The filter output peaked up over potential targets as expected, reducing ambiguity in the exact location of targets. The data used for the matched filter autoprocessor demonstration was magnetometer array data from the vehicular *MTADS* surveys at JPG TD. The magnetometers were spaced 0.25 m apart, so surface coverage was not 100%. We expected that small objects, such as 20-mm projectiles, could pass between the magnetometers without being detected, while large objects buried more deeply would more likely be detected.

The ground truth for JPG TD Area 3 lists a total of 20 UXO and 35 OE. The UXO were:

20 mm projectiles	4
57 mm, 60 mm	5
2.75 in	1
76 mm	1
81 mm	4
105 mm	1
152 mm	1
155 mm.	1

Table 4 shows the detection dig list results for Area 3. Of the 20 seeded UXO, the MFAP dig list contained 16 as possible ordnance to be dug, and did not list any of them as clutter. The missing ordnance are three of the four 20 mm targets and one 81 mm target. The percentage of the to-be-dug items that were in fact nonordnance was large (83%), as expected, since the magnetometer array and matched filter analysis provide detection, but only a limited discrimination capability.

Table 4. Matched Filter AutoProcessor Dig List Results for JPG TD Area 3.

Targets Detected	Targets Buried	UXO Detections and Pd	Probability of Detection	UXO Not Detected	Probability of False Alarm
20 mm assumed present	55 20 UXO 35 OE	16 of 20	80%	3 (20 mm) 1 (81 mm)	83%
no 20 mm assumed present	55 16 UXO 39 OE	15 of 16	94%	1 (81 mm)	83%

It is clear that the relatively low detection rate (80%) is mostly due to problems detecting the 20 mm targets.

Of the three non-detected 20 mm targets:

- the first was located in a data gap at even the shallowest chosen filter depth of 0.10 m and was not found by the matched filter
- the second was found by the matched filter but screened out because it had a low data/model coherence (0.55, the threshold was 0.80)
- the third was not found by the matched filter, and was not seen when the data was inspected visually.

The missed 81 mm was found by the matched filter peak finder. However, it was at the edge of a data gap; this reduced the data/model coherence to 0.74, falling below the threshold because a substantial part of its signature was in the data gap and could not be fit.

Table 5 shows the accuracy of the target locations compared to the ground truth for JPG TD Area 3.

Table 5. Horizontal Position and Depth Differences between Detected UXO and Ground Truth for JPG TD Area 3.

	Horizontal Difference (m)	Depth Difference (m)
average	0.10	0.14
median	0.09	0.11

4.3 TECHNOLOGY COMPARISON

Our dig lists for all three JPG TD areas, as well as the ground truth for Area 3 (provided by George Robitaille of the U.S. Army Environmental Center), are appendices in the Final Report[13], but the MFAP target detections and dig list are compared with the ground truth and with the results of other UXO detection systems and analyses below.

Table 6 shows the detection probabilities and false alarm counts for MFAP and U-Hunter analyses. These results are shown graphically in Figure 7, along with the Receiver Operating Characteristics (ROCs) for the primary demonstrators using electromagnetic induction (EMI) systems. The three colored points on each plot indicate the relative performance of analysis of magnetometer data using the MFAP and U-Hunter, as well as standard Mag and Flag methodology. U-Hunter and Mag and Flag points generally lie far to the right of the curves, indicating significantly poorer performance. The MFAP points, on the other hand, reveal performance comparable to the best demonstrators in Area 2, and intermediate between the various demonstrators in Areas 1 and 3.

Table 6. Detection Probabilities and False Alarm Counts for U-Hunter and MFAP Analyses for JPG TD 2000.

	U-Hunter		MFAP	
	Pd	**false alarms**	**Pd**	**false alarms**
Area 1	0.72	165	0.55	52
Area 2	0.7	200	0.6	62
Area 3	0.65	124	0.65	78

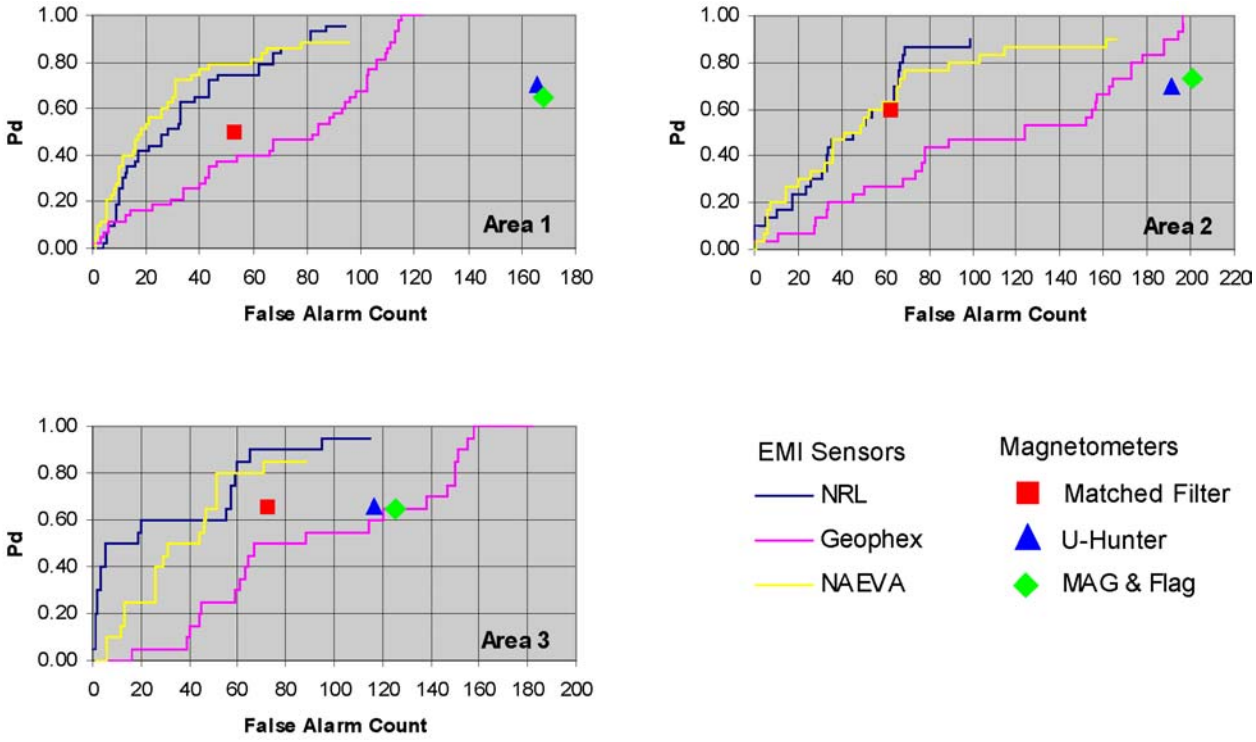

Figure 7. ROC Curves for JPG TD Tested Systems (NRL, Geophex and NAEVA) and Detection Statistics for Three Magnetometer Analysis Methods (MFAP, U-Hunter, MAG & Flag).

5.0 COST ASSESSMENT

5.1 TIME AND EXPERIENCE EVALUATION

We investigated the ease of use of the MFAP, in terms of how much operator training is necessary to obtain optimal results. An operator with no previous experience with magnetic systems and no technical knowledge of ordnance detection systems was given about 20 minutes of basic training on running the MTADS DAS and picking targets from magnetometer data. He then used the DAS to analyze Area 3 of JPG TD. The results are shown in Table 7. There was a learning curve for picking targets with the DAS; he analyzed the data three times (Trials 1, 2 and 3), picking more targets each time, as shown in the table.

This operator then was given a brief training (15 minutes) on how to run the MFAP, for which he used all default values for thresholds and just ran the peak picker. (The raw data had previously been filtered at 12 depths.) He ran the peak picker on these 12 depths. Finally, he ran the peak picker on the 5 depths (described in section 4.1) that had been analyzed previously by an experienced operator. The inexperienced operator achieved a 75% (MFAP) or 80% (*MTADS* DAS) detection rate.

These results are compared in Table 7 to those of an experienced operator using both the *MTADS* DAS and the MFAP. The experienced operator using *MTADS* found all targets except one 20 mm, and using MFAP found all targets except two 20 mm. Using the MFAP, the experienced operator did more than autoprocess; he ran the automatic peak finder but then examined the images to decide if any dipole-like targets were missed. He still missed an additional 20 mm compared to *MTADS* because it was lying very near a data gap. (This weakness of the MFAP is discussed further in Section 6.0.)

Note that detection rates in Table 7 refer to targets identified in the first data analysis, before screening. The final dig list excludes some of these detected targets because of low data/model coherence (due to data gaps).

We also investigated the processing and analysis times for the Matched Filter AutoProcessor and compared it to analysis times using the *MTADS* Data Analysis System (DAS). Our experience with the existing automatic processor in the *MTADS* DAS is that it can process 5 to 10 acres per hour of magnetometer array data, depending on the threshold and target density.[19] By comparison, a human operator can process about 1 acre per hour in the user-interactive mode at the same target density. The analysis time using the *MTADS* DAS is shown below in Table 8 for the inexperienced operator's third trial (refer to Table 7). Although the Matched Filter Autoprocessor (MFAP) data analysis of JPG TD was performed in AETC's offices and not in the field, we tracked the processing times for the various steps involved in the MFAP: running the filter at a given depth and selecting the peaks. These are shown in Table 8. Note that the Pre-Processing Times are for computations run completely automatically, without any required operator intervention or presence. The analysis times are for comparable operator effort.

Table 7. MFAP and *MTADS* Performance (before attribute screening) **by Inexperienced and Experienced Operators on Area 3 of JPG TD, Assuming 20 mm Ordnance Was Present.**

Analysis System	# of targets picked	ordnance detected	Inexperienced Operator		Experienced Operator	
			ordnance missed	Pd	ordnance missed	Pd
MTADS DAS, Trial 1	68	12 of 20	4 20mm 1 81 mm 2 60 mm 1 155 mm	65%	1 20 mm	95%
MTADS DAS, Trial 2	128	16 of 20	3 20 mm 1 81 mm	80%	1 20 mm	95%
***MTADS* DAS, Trial 3**	144	16 of 20	3 20 mm 1 81 mm	**80%**	1 20 mm	**95%**
MFAP (12 depths)	1091	15 of 20	2 20 mm 1 81 mm 2 60 mm	**75%**	2 20 mm	**90%**
MFAP (5 depths)	561	14 of 20	3 20 mm 1 81 mm 2 60 mm	70%	2 20 mm	90%

Table 8. Processing Times for an Inexperienced Operator Using the *MTADS* DAS and MFAP Analysis Systems on Data from Area 3 of JPG TD.

Analysis System	Pre-Processing Time* (min)	Analysis Time** (min)
***MTADS* DAS**	n/a	105
MFAP (12 depths)	491	50
MFAP (5 depths)	166	20

* The pre-processing time is the time to run the matched filter on the raw data for all selected depths to produce the matched filter output images. This time is both filter-depth dependent and computer-platform dependent. On the computer at AETC, it took 9 minutes for the shallowest depth and 88 minutes for the deepest depth.

** The analysis time is the time to operate the automatic peak finder on the matched filter output image.

6.0 IMPLEMENTATION ISSUES

A number of issues appeared during the development and testing of the MFAP. Some were solved; others were beyond the scope of the project. Both types are listed below, along with solutions found or suggestions for the future.

(1) The CDF threshold/contouring procedure used for automated target picking, which worked on the previous sites, produced an overwhelming number of spurious targets when applied to the JPG TD data. We decided that using the Cumulative Distribution Function of the filter output over an entire image was a major cause of the problem. Calculating CDFs and picking targets over smaller sub-areas of an image has eliminated this problem and the target-picking algorithm has been appropriately modified.

(2) The matched filter procedure is sensitive to survey defects that produce missing data. Several UXO targets were not detected or included in the dig list because of the expansion of areas of missing data with increasing filter depth. One solution might be to relax the data/model coherence threshold for objects very near the edge of data gaps.

A solution to the problem of data lost at the edges of the survey region is to survey outside the search area. Since the filter box width for a filter depth of 3.5 m is 14 m, one would need to survey at least 7 m beyond the edges of the UXO search area to avoid missing targets as deep as 3.5 m (a 7.7 m border region is required for 4 m deep targets).

For interior gaps, man portable systems will decrease the gaps but not eliminate them. One can, however, interpolate from the edges of an interior gap towards its center so that the data is filled in. Obviously, any interpolation scheme must give reasonable results across these gaps or we risk trading the problem of missing data for that of spurious or non-physical data. To develop a reasonable interpolation procedure, gaps of exactly the same size and shape as real regions of missing data should be introduced into areas where we do have data. We can then compare interpolated results with the original removed data to see which interpolation procedures best reproduce the original. This scheme has not been developed in this project.

(3) When we compared Area 3 results with the ground truth, we found we were too conservative in setting our dig/no-dig boundary of fitted dipole orientation; this was changed for the analysis of the other two areas.

(4) Operating the MFAP on magnetometer array data provides less discrimination capability than operating on active electromagnetic data. Incorporation of the matched filter into active EM data analysis systems should provide further screening criteria and thus better performance.

This page left blank intentionally.

7.0 REFERENCES

1. Office of the Undersecretary of Defense (Acquisition and Technology), "Report to Congress: Unexploded Ordnance Clearance," March 27, 1997.

2. Office of the Undersecretary of Defense (Acquisition and Technology), "Report of the Defense Science Board Task Force on Unexploded Ordnance (UXO) Clearance, Active Range Clearance, and Explosive Ordnance Disposal (EOD) Programs, April 1998.

3. "UXO Technology Demonstration Program at Jefferson Proving Ground (Phase III)," U.S. Army Environmental Center Report No. SFIM-AEC-ET-CR-97011, April 1997.

4. "Unexploded Ordnance Advanced Technology Demonstration Program at Jefferson Proving Ground (Phase II)," U.S. Army Environmental Center Report No. SFIM-AEC-ET-CR-96170, June 1996.

5. Pederson, A. and B. Stalcup, "Phase III Advanced Technology Demonstrations at Jefferson Proving Ground," UXO Forum '97, Nashville, Tennessee, May 28-30, 1997, Conference Proceedings pp. 281-289.

6. Burgess, A.E., L. Xing and C.K. Abbey, "Visual Signal Detectability with Two Noise Components: Anomalous Masking Effects," *J. Opt. Soc. Am.* A, Vol. 14, No. 9, Sept. 1997, pp. 2420-2442.

7. Rolland, J.P. and H.H. Barrett, "Effect of Random Background Inhomogeneity on Observer Detection Performance," *J. Opt. Soc. Am.* A, Vol. 9, No. 5, May 1992, pp. 649-658.

8. Eckstein, M.P., A.J. Ahumada and A.B. Watson, "Visual Signal Detection in Structured Backgrounds. II. Effects of Contrast Gain Control, Background Variations, and White Noise," *J. Opt. Soc. Am.* A, Vol. 14, No. 9, September 1997, pp. 2406-2419.

9. Rohaly, A.M., A.J. Ahumada and A.B. Watson, "Object Detection in Natural Backgrounds Predicted by Discrimination Performance and Models," *Vision Research*, Vol. 37, 1997, pp. 3225-3235.

10. Kassam, S.A. and H.V. Poor, "Robust Techniques for Signal Processing: A Survey," *Proc. IEEE*, Vol. 73, No. 3, March 1985, pp. 433-481.

11. van Trees, H.L., *Detection, Estimation and Modulation Theory, Part 1*, John Wiley and Sons, 1968, Sect. 2.4.2.

12. "Advanced UXO Detection/Discrimination, Technology Demonstration, U.S. Army Jefferson Proving Ground, Madison, Indiana," Technology Demonstration Plan, Naval Explosive Ordnance Disposal Technology Division (NAVEODTECHDIV), 30 June 2000.

13 Bell, T., R. Jones, J. Soukup and B. Puc, "Matched Filter Processor for Detection and Discrimination of Unexploded Ordnance," AETC Final Report VA-095-050-TR-01, Revised and Finalized 26 November 2001.

14. Barrow, B., R. DiMarco, N. Khadr and H.H. Nelson, "Processing and Analysis of UXO Signatures Measured with *MTADS*," UXO Forum '97, Nashville, Tennessee, May 28-30, 1997, Conference Proceedings pp. 8-18.

15. Bell, T., "Looking for a Perfect Match: Model-based Characterization Fits Data to UXO Signatures", *Ordnance Explosives Environment*, Vol. 4, No. 2., April-June 1997, p. 5.

16. Altshuler, T. W., "Techniques for False Alarm Mitigation to Improve Magnetic Detection of Unexploded Ordnance," Third Annual SERDP Symposium, Washington, D.C., December 3-5, 1997.

17. Altshuler, T.W., "Shape and Orientation Effects on Magnetic Signature Prediction for Unexploded Ordnance," UXO Forum '96, Williamsburg, Virginia, March 26-28, 1996, Conference Proceedings pp. 282-291.

18. McDonald, J.R., "*MTADS* UXO Surveys at the Badlands Bombing Range," Third Annual SERDP Symposium, Washington, D.C., December 3-5, 1997.

19. Barrow, B.J., "Report on *MTADS* Automatic Processor," AETC Report VA-074-075-TR, January 12, 1998.

APPENDIX A

POINTS OF CONTACT

Jeffrey Marqusee
ESTCP Director
901 North Stuart St.
Suite 303
Arlington, VA 22203
Telephone: (703) 696-2120
Fax: (703) 696-2114
E-mail: marqusj@acq.osd.mil

George Robitaille
DoD Project Officer
Army Environmental Center
SFIM-AEC-ETD
Aberdeen Proving Ground, MD 21010-5401
Telephone: (410) 436-6865
Fax: (410) 436-6836
E-mail: gerobita@aec.apgea.army.mil

Thomas Bell
Principal Investigator
AETC, Inc.
Suite 800
1225 Jefferson Davis Highway
Arlington, VA 22202
Telephone: (703) 413-0500
Fax: (703) 413-0512
E-mail: tbell@va.aetc.com

APPENDIX B

OASIS MONTAJ INTEGRATION

B 1.0 OASIS MONTAJ INTEGRATION OVERVIEW

The matched filter algorithm, which was originally codified in the Interactive Data Language (IDL; Research Systems, Inc.), implements optimal linear filtering in a threshold-based UXO detection scheme. Following successful demonstration of the approach, the algorithms were recoded to seamlessly integrate with OASIS Montaj. OASIS Montaj is developed and marketed commercially by Geosoft, Inc., and includes a very large capacity database, a graphical user interface, and a plethora of geophysical processing and mapping routines.

As described above, the matched filter processor convolves a dipole-based model signature with a gridded (or krigged) approximation of the measured data. As such, the inputs include the gridded data file, geographic information regarding the site (required in order to calculate the inclination and declination of the Earth's magnetic field), the size of the filter box (described below), and the distance between the sensors and the ground's surface. The outputs include a filtered output grid and an OASIS Montaj database containing the output grid data, spatial locations, and model parameters.

There are three basic steps involved with the OASIS Montaj matched filter executable. First, the input data are submitted to the filtering routine by calling a Geosoft executable ('matchfilter.gx'). The 'matchfilter.gx' interfaces with the OASIS Montaj database and passes the data to a dynamic link library that creates the filter output grid and model parameters. The second step involves refining the filter output (if desired) by utilizing the model parameters. In the third step, peaks are identified in the final data to create the anomaly list.

Figure B-1 shows the user dialogue window that is displayed upon calling the Geosoft executable ('matchfilter.gx'). Geosoft executables are processes that perform a variety of data processing tasks. Required inputs for the matched filter executable include an OASIS Montaj grid file, the sensor offset (distance between the ground's surface and the magnetic sensors), the base length of the filter box, the latitude and longitude of the site, and geomagnetic reference field information. The 'Output Grid File' requests a filename for the matched filter output results. A database containing all measured data and fit results (or model parameters) is also created using the same name but with a *.gdb extension.

Similar to the previously prototyped IDL code, a filter box is created around each point (x_0, y_0) in the grid. The model signal in the matched filter is a dipole located at the center of the filter box (x_0, y_0) for various depths, plus a linear magnetic background field. A multiple linear regression on the data for all points in the box yields the best-fit signal model dipole and the background field constants.

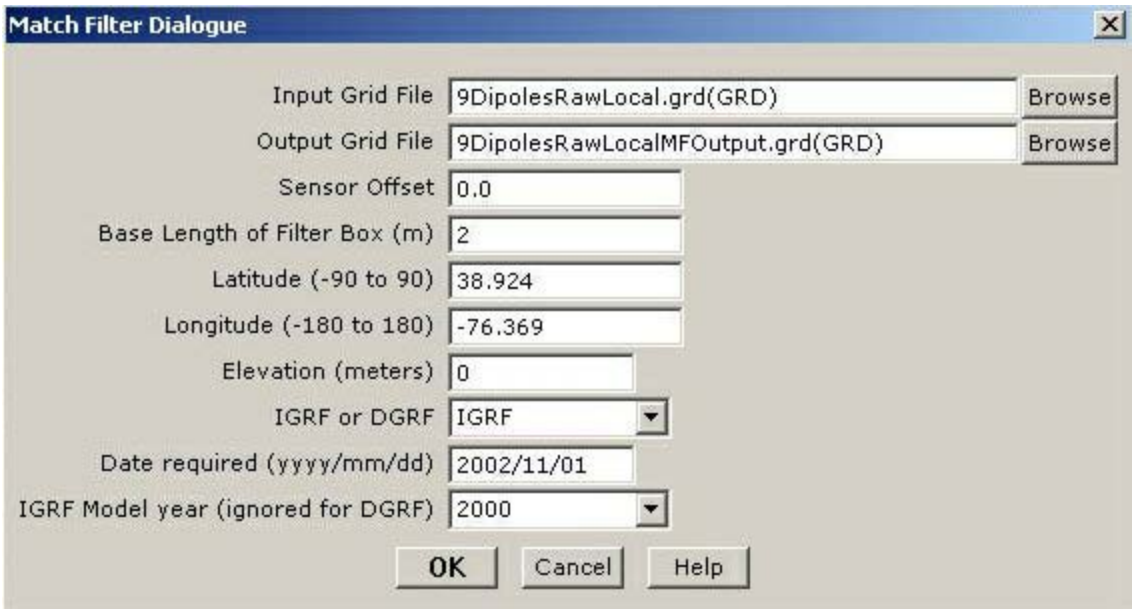

Figure B-1. Screen snapshot of the Matched Filter Dialogue box.

The OASIS Montaj version of the Matched Filter searches over six target depths (0.25m, 0.5m, 0.75m, 1.0m, 1.25m, and 1.5m). The depth that produces to the best fit (i.e., lowest error in terms of model minus measured data) is selected, and the model parameters for that depth are stored. An additional modification was made regarding the size of the filter box. In the IDL prototype code, the size of the filter box was a function of the user-selected interrogation depth. It was concluded, however, that the matched filter output was not sensitive to the size of the filter box. In the OASIS Montaj version, the size of the filter box is assigned by the user and is not a function of the interrogation depth.

As part of the JPG TD program, the NRL surveyed the three prepared areas using the vehicular Multisensor Towed Array Detection System (*MTADS)* magnetometer arrays. These data were preprocessed by the NRL to create geo-referenced mapped data files. The *MTADS* magnetometer data from Area 1 was analyzed using the matched filter routine developed for the OASIS Montaj environment.

B 2.0 OASIS MONTAJ FILTER PERFORMANCE

B 2.1 SYNTHETIC DATA

Synthetic data, created using forward models, were used to evaluate the OASIS Montaj-embedded matched filter routine. Table B-2 provides details regarding the location and characteristics of magnetic dipoles while Figure B-2 presents a color-coded contoured representation of the synthetic data. The synthetic data contain nine distinct dipoles, each with a unique combination of depth, location, and orientation.

Table B-2. Location and Characteristics of Magnetic Dipoles for Synthetic Data

ID	X (m)	Y (m)	Depth (m)	Inc (deg)	Dec (deg)	Size (m)
1	10	10	0.5	0	0	0.05
2	20	10	0.5	0	90	0.05
3	30	10	0.5	0	180	0.05
4	10	20	0.5	30	0	0.05
5	20	20	1.5	30	90	0.10
6	30	20	0.5	30	180	0.05
7	10	30	0.5	60	0	0.05
8	20	30	0.5	60	90	0.05
9	30	30	0.5	60	180	0.05

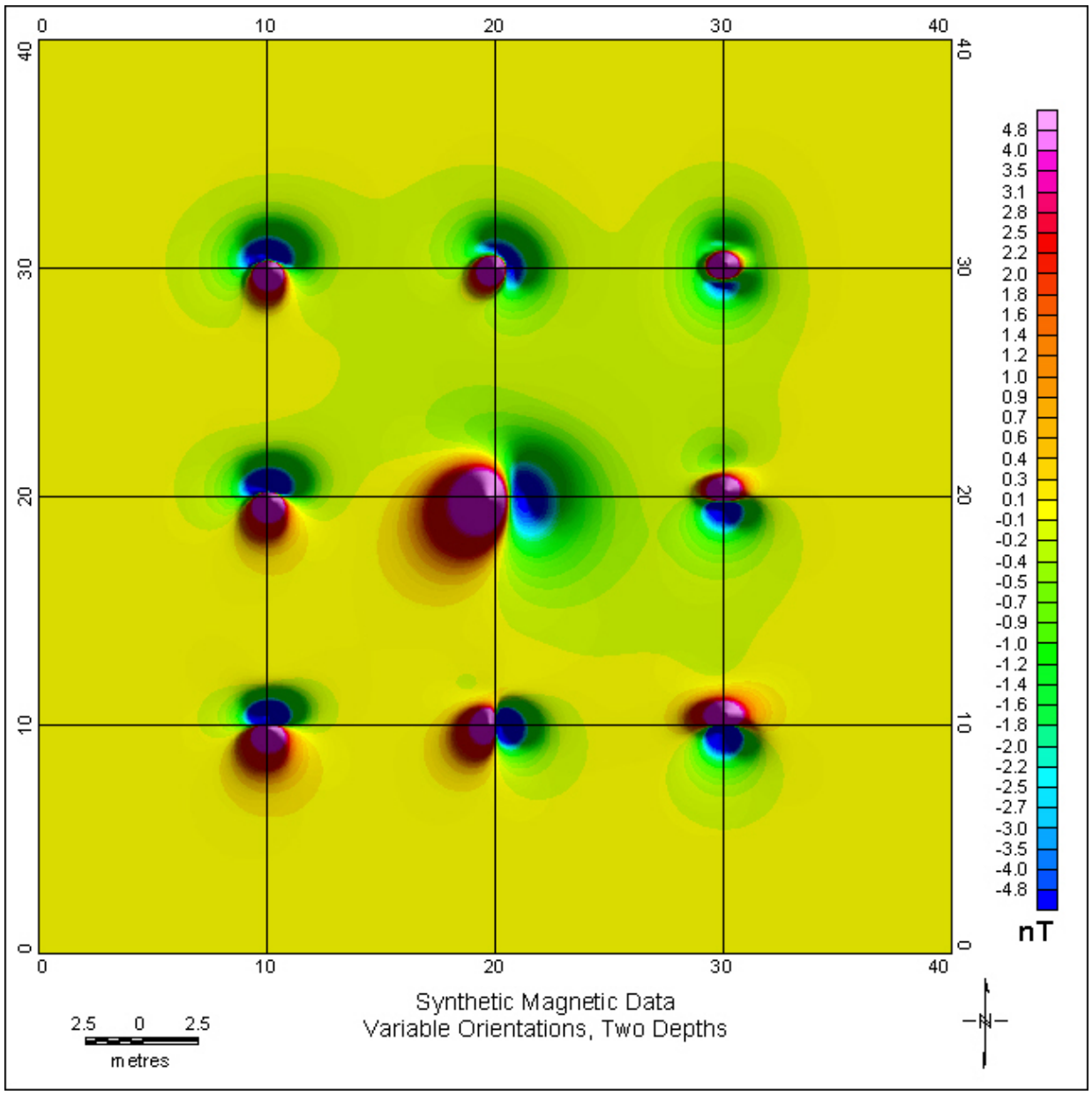

Figure B-2. Color-coded map of synthetic data used to test the matched filter routine.

The matched filter output data, shown in Figure B-3, clearly indicate the presence of nine dipoles. Processing artifacts are also apparent. The artifacts occur when the filter window contains only a portion of the dipolar signal (typically a single positive or negative lobe) that is associated with the causative source. When this happens, the filter incorrectly creates the missing lobe, which produce erroneous output values. These artifacts were present in the IDL prototyped code as well.

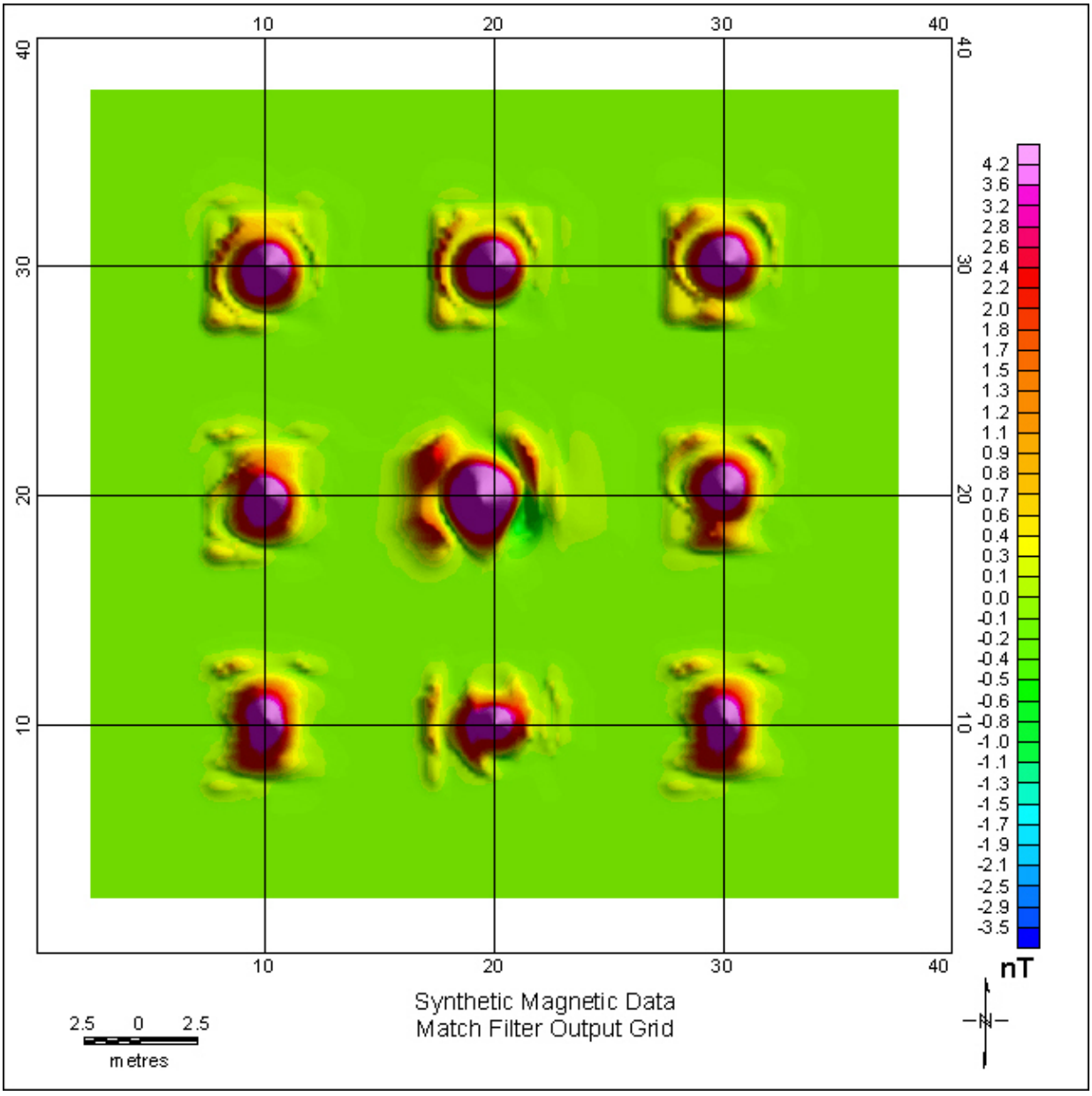

Figure B-3. Color-coded map showing results of the OASIS Montaj Matched Filter.

The OASIS Montaj matched filter stores the filter results and all derived model parameters in a database. The model parameters can be used to refine the filter output. Figure B-4 shows, in profile form, the matched filter output ('MFoutput'), the model error ('Chisq'), and the ratio ('MFoutput/Chisq'). When the filter window coincides with the center of a dipolar signal, the error term is dramatically reduced. In other words, the derived model closely matches the input (measured or synthetic) data when it is directly on top of the center of the dipole. The horizontal axis in Figure B-4 represents the sample number (or fiducial). For reference, fiducial number 12,960 coincides with x=20, y=20 in Figures B-2 and B-3. There are three major groupings in Figure B-4 - each with multiple local peaks. The left-most grouping represents data along y=19.75m. The center grouping represents data along y=20.0 meters, and so on. Within the center grouping (y=20.0 meters), there are three peaks in the MFoutput channel (blue) – each peak represent one of the three dipoles located at x=10-, 20-, and 30-meters.

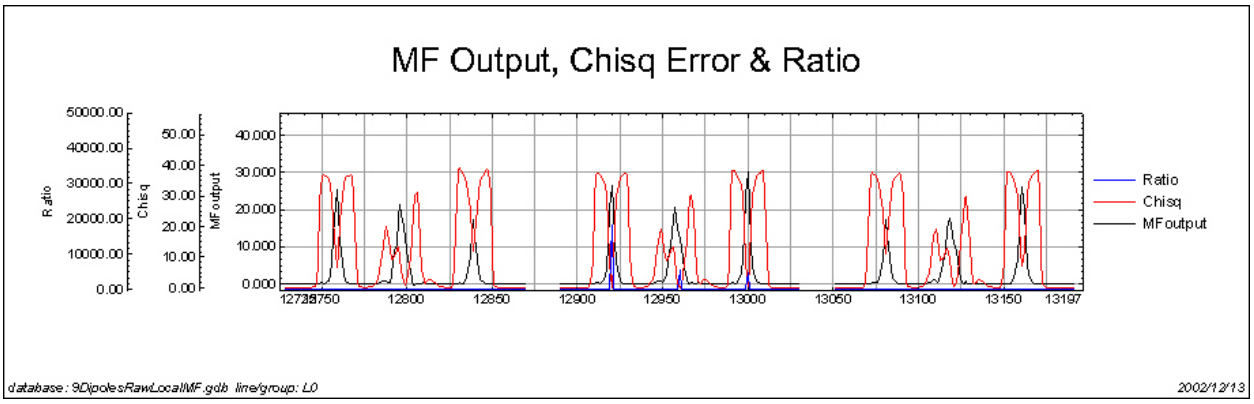

Figure B-4. Profile view of the Matched Filter output and Error term. Fiducial number 12,960 corresponds to x=20, y=20 in Figures B-2 and B-3. Note that the error term ('Chisq') is minimized when the filter output 'MFoutput' is maximized. In other words, when the center of the filter box coincides with a dipole source, the model data closely match the synthetic data.

Figure B-5 shows the results of dividing the matched filter output by the error term. As observed in the figure, the anomalies possess a very high signal-to-noise ratio and the processing artifacts are reduced.

The derived model parameters for these synthetic data are shown in Table B-3. Because the OASIS Montaj version of the matched filter routine includes searches over multiple depths, the anomaly depth estimates are reasonable. Comparing Tables B-2 and B-3 reveals that the size, depth, inclination, and declination estimates are, in fact, quite good.

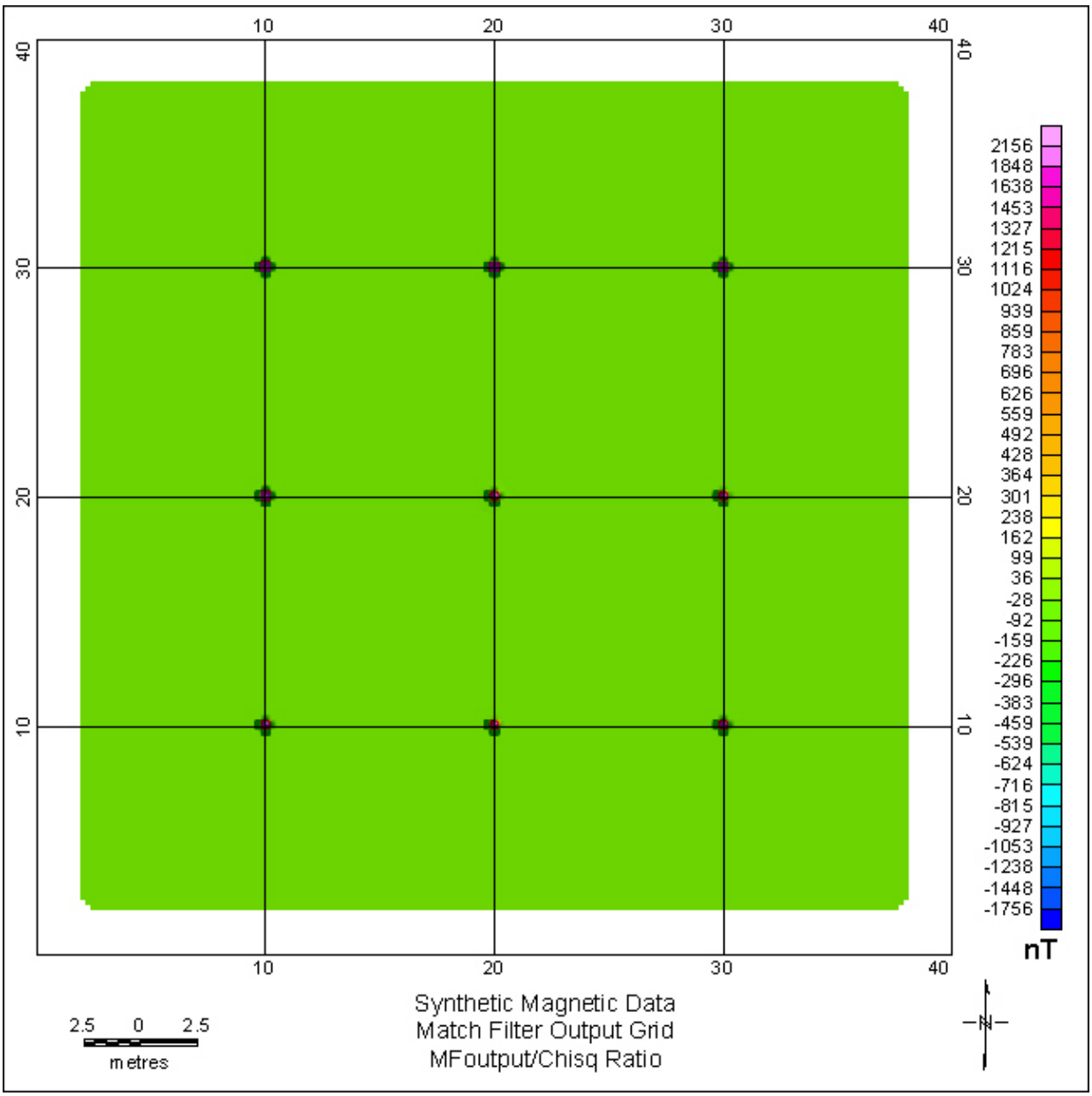

Figure B-5. Color-coded map of the matched filter output divided by the error term.

Table B-3. Matched Filter Results and Derived Model Parameters

ID	X (m)	Y (m)	Depth (m)	Inc (deg)	Dec (deg)	Size (m)
1	10	10	0.5	0.5	0.1	0.05
2	20	10	0.5	-0.3	90.0	0.05
3	30	10	0.5	-0.5	180.0	0.05
4	10	20	0.5	30.7	0.5	0.05
5	20	20	1.5	29.6	90.6	0.10
6	30	20	0.5	29.4	179.4	0.05
7	10	30	0.5	61.0	1.3	0.05
8	20	30	0.5	59.3	91.5	0.05
9	30	30	0.5	59.2	178.7	0.05

B 2.2 Jefferson Proving Ground Magnetic Data – Area 1

Magnetic data from Area 1, JPG TD, were run through the OASIS Montaj-embedded matched filter to compare with results obtained using the IDL prototyped code. The Naval Research Laboratory acquired the magnetic data using the vehicular *MTADS* platform. Seeded UXO ranged in size from 20-mm aircraft-fired projectiles to 155-mm howitzer projectiles. Figure B-6 shows the sensor track density for this site.

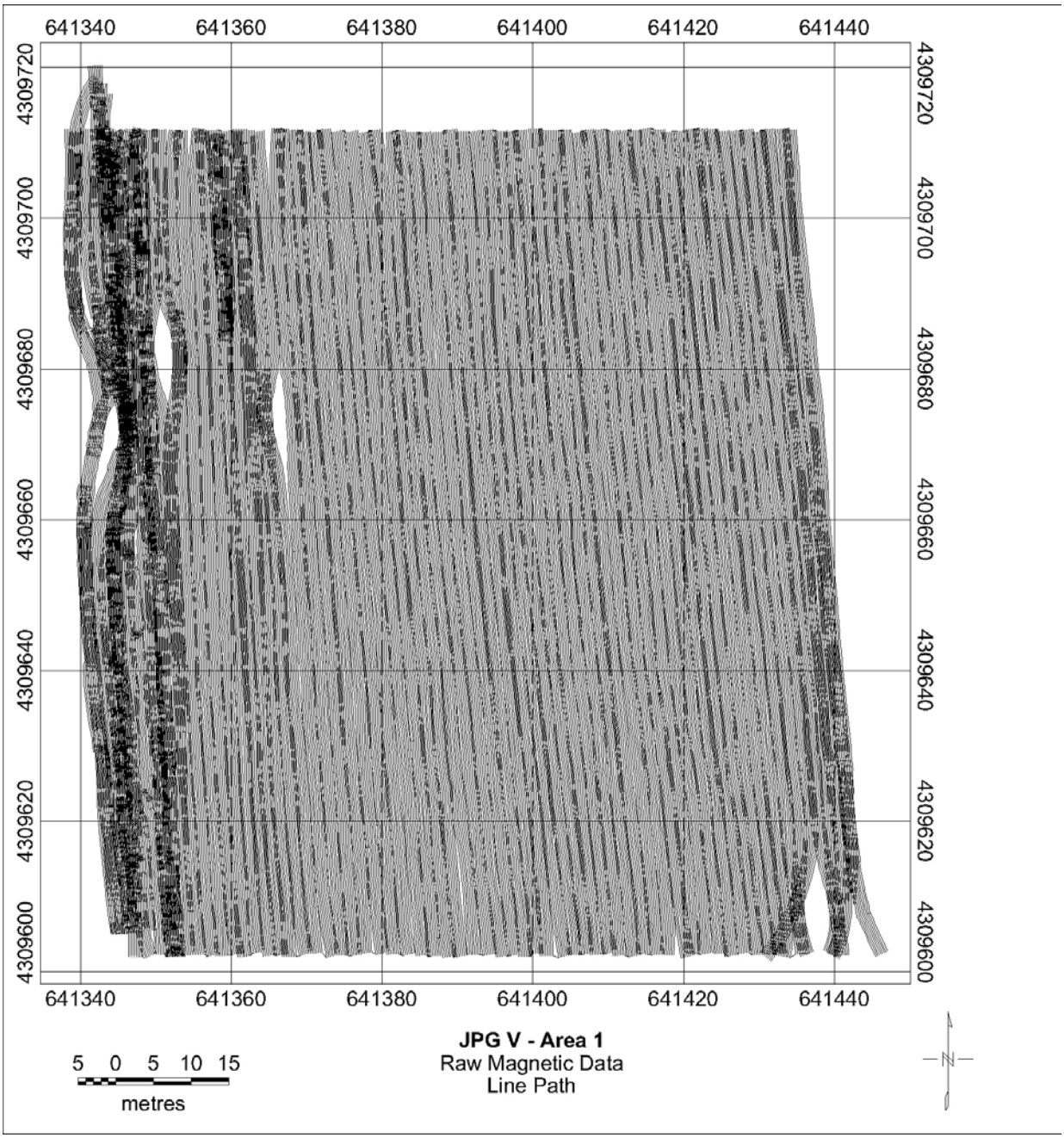

Figure B-6. Area 1 from JPG TD – sensor track density.

The data gaps, which are indicated in Figure B-6 by holes in the sensor track density, create problems for the matched filter algorithm. The default gridding process used to create the map shown in Figure B-7, for example, did not allow the gaps to be interpolated. These data gaps in the gridded data will be enlarged by one-half the size of the filter window during the matched filtering process. As a result, anomalies near the margin of data gaps will be missed if the data gaps are not interpolated during the gridding process.

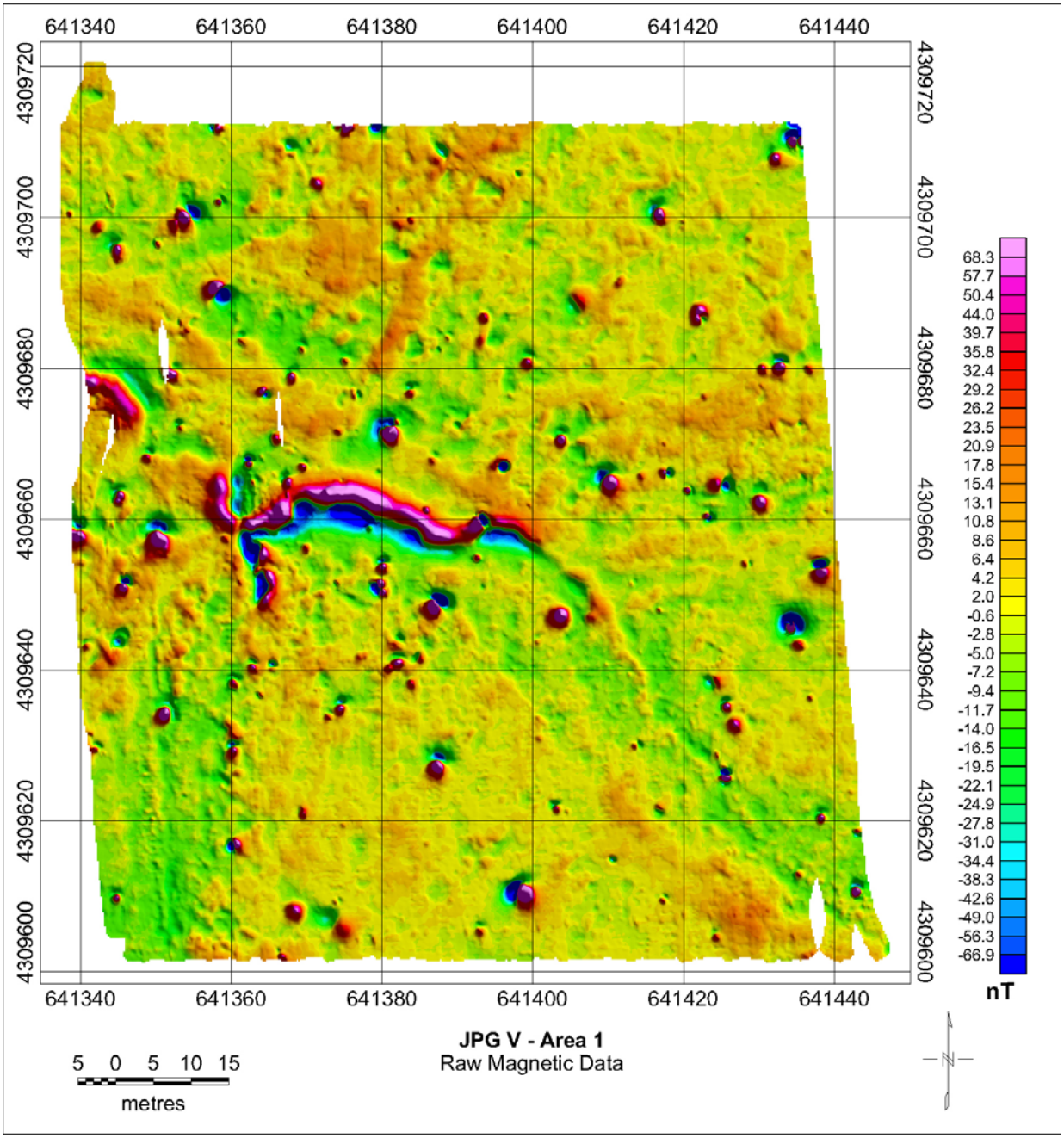

Figure B-7. Color-coded map of the *MTADS* magnetic data, Area 1 JPG TD.

By allowing data gaps to be interpolated during the gridding process, the problems associated with data gaps are eliminated. OASIS Montaj allows the user to define the distance over which grid values are interpolated. Figure B-8 presents a map of Area 1 with the data gaps filled in (i.e., interpolated) during gridding.

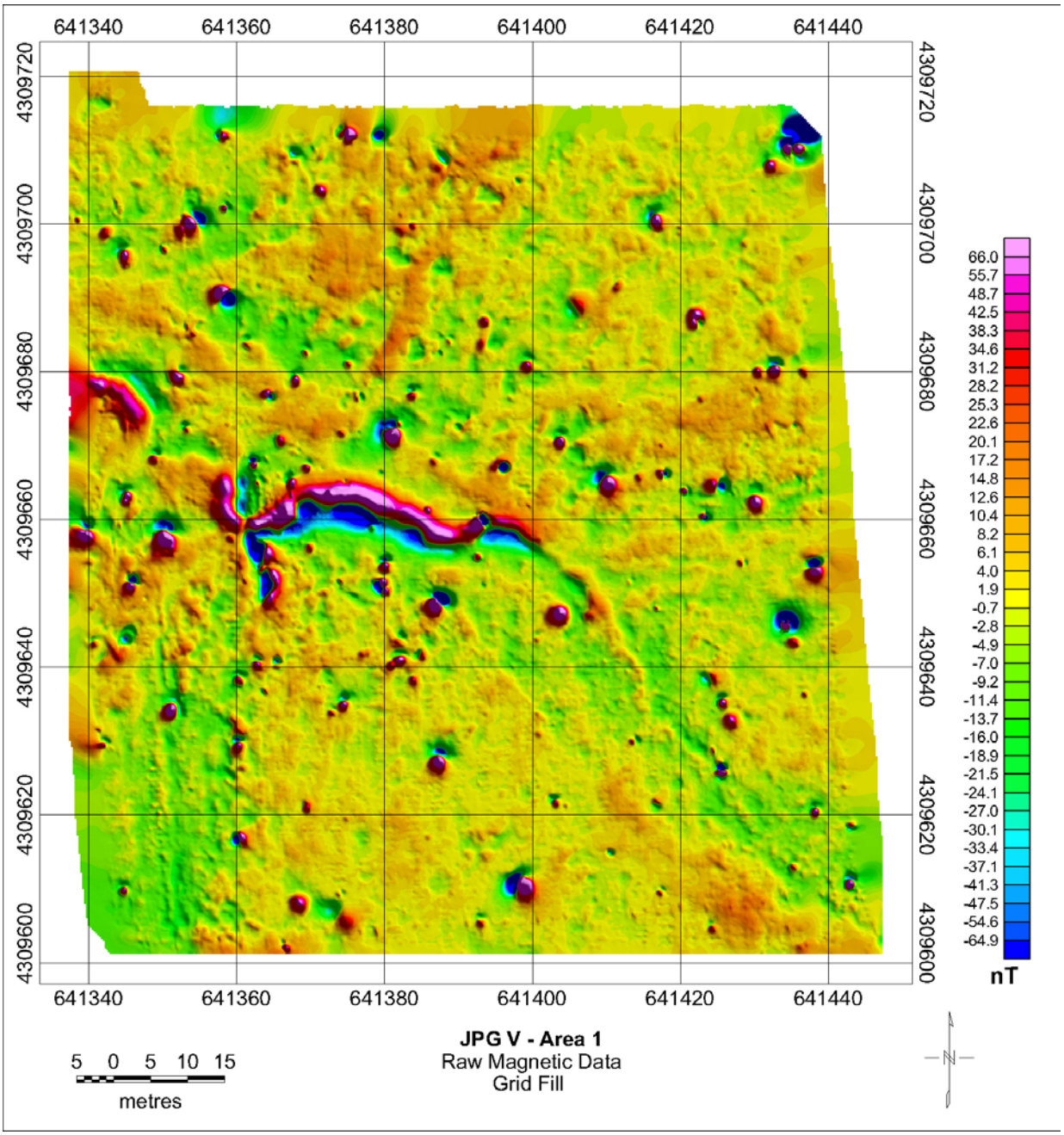

Figure B-8. Color-coded map of the *MTADS* magnetic data, Area 1 JPG TD. Note that the data gaps apparent in Figures B-6 and B-7 have been interpolated.

Figures B-9 through B-16 present results of the OASIS Montaj matched filter data from Area 1. The various maps are derived from the database that contains the filter output and model parameters that were derived during filtering.

The series of maps and the associated logic presented below differs from the IDL prototyped matched filter procedures. The IDL prototyped matched filter algorithm did not search over multiple depths and did not store the model parameters. Instead, the filter algorithm was repeatedly run at various depths and the derived filter images were each examined for peaks (i.e., anomalies). The anomaly lists were subsequently combined into a master list. Once the master anomaly list was created, the measured data (not the gridded data) around each anomaly location was submitted to a dipole-estimating algorithm. The dipole-estimating algorithm analyzed each target and stored the best fitting model parameters. The anomalies were then screened and sorted based upon the derived model parameters.

The process presented herein basically tries to enhance or retain anomalies that are observed in the raw magnetic data while reducing or eliminating those features that are not associated with expected signatures. All of the model parameters were derived from the gridded approximation of the measured data.

Figure B-9 presents the matched filter output of Area 1, JPG, without any post processing. As observed in the figure, a number of anomalies possess very large amplitudes while others do not appear to be caused by an isolated item (i.e., they are not localized and appear to be related to the background geology – compare Figures B-8 and B-9).

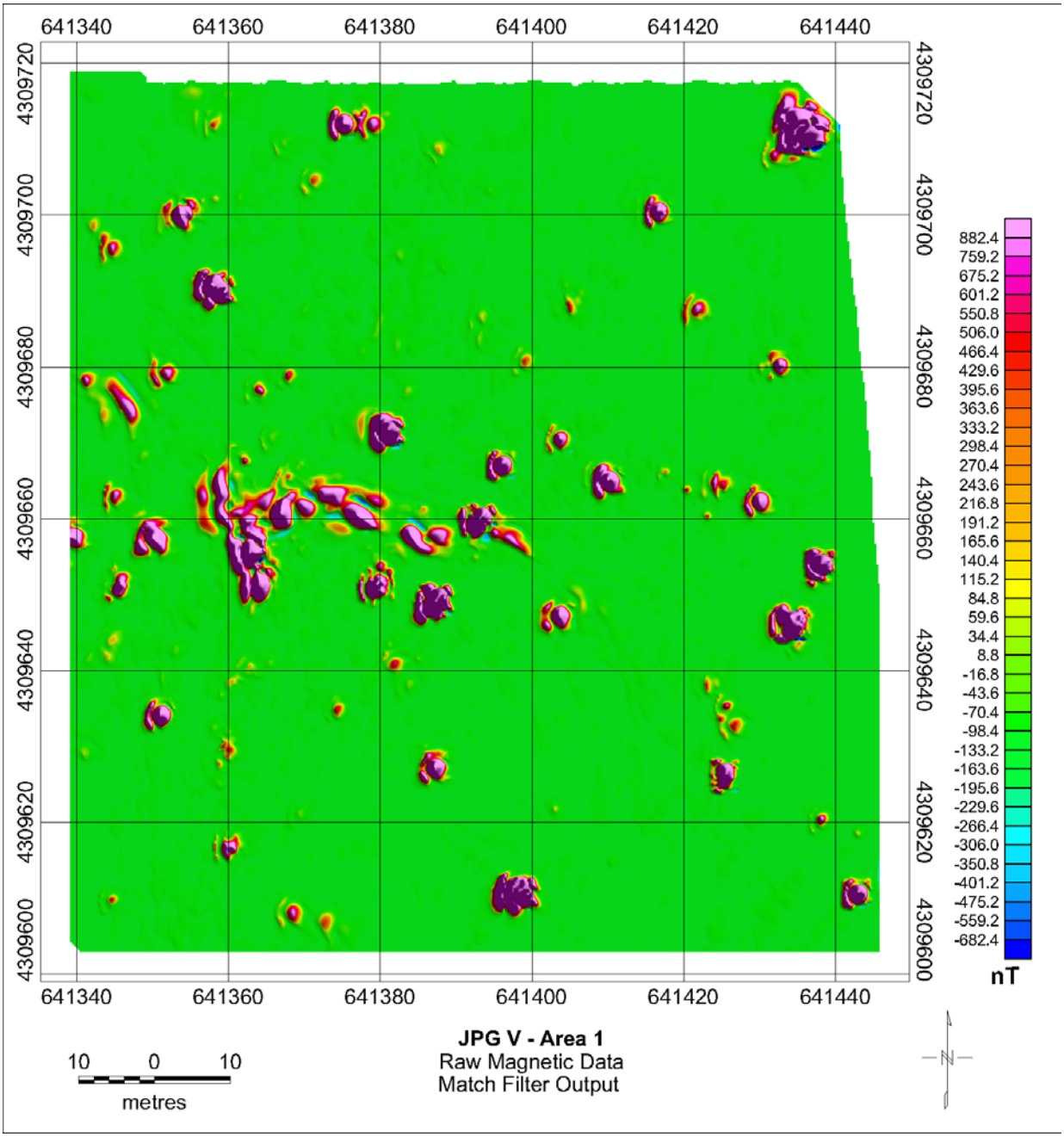

Figure B-9. Color-coded map showing the results of the matched filter, Area 1 JPG TD.

Figure B-10 presents the ratio of the matched filter output and the derived model error term. This 'ratio' map is notably different in nature than that shown in Figure B-9. Unlike the noise-free synthetic data case presented earlier, the presence of complicated structures in the measured response associated with nearby targets, clutter, or geologic sources produces numerous potential targets.

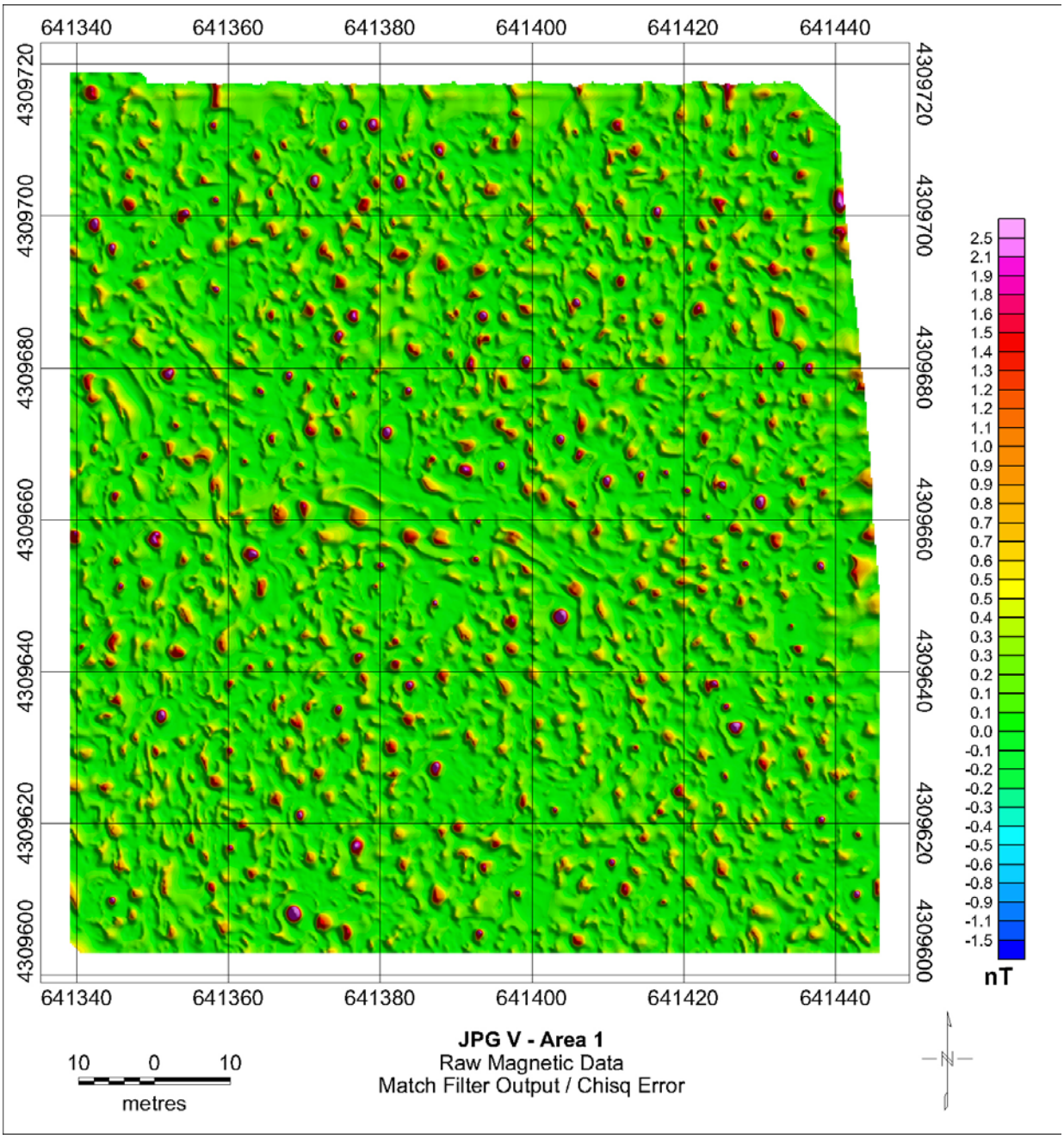

Figure B-10. Color-coded map showing the results of dividing the matched filter output by the derived model error; Area 1 JPG TD.

Based on a visual inspection of the filter output and raw data, it was noted that realistic anomalies observed in the raw data also had filter output values larger than five. Figure B-11 presents the ratio of the matched filter output and the derived model error term for those filter values that are greater than five. [Note: The output filter values depend on the filter box size – a filter box with a base length of 3.75m was used for this example. It is incorrect to assume that different data sets should apply the same threshold.]

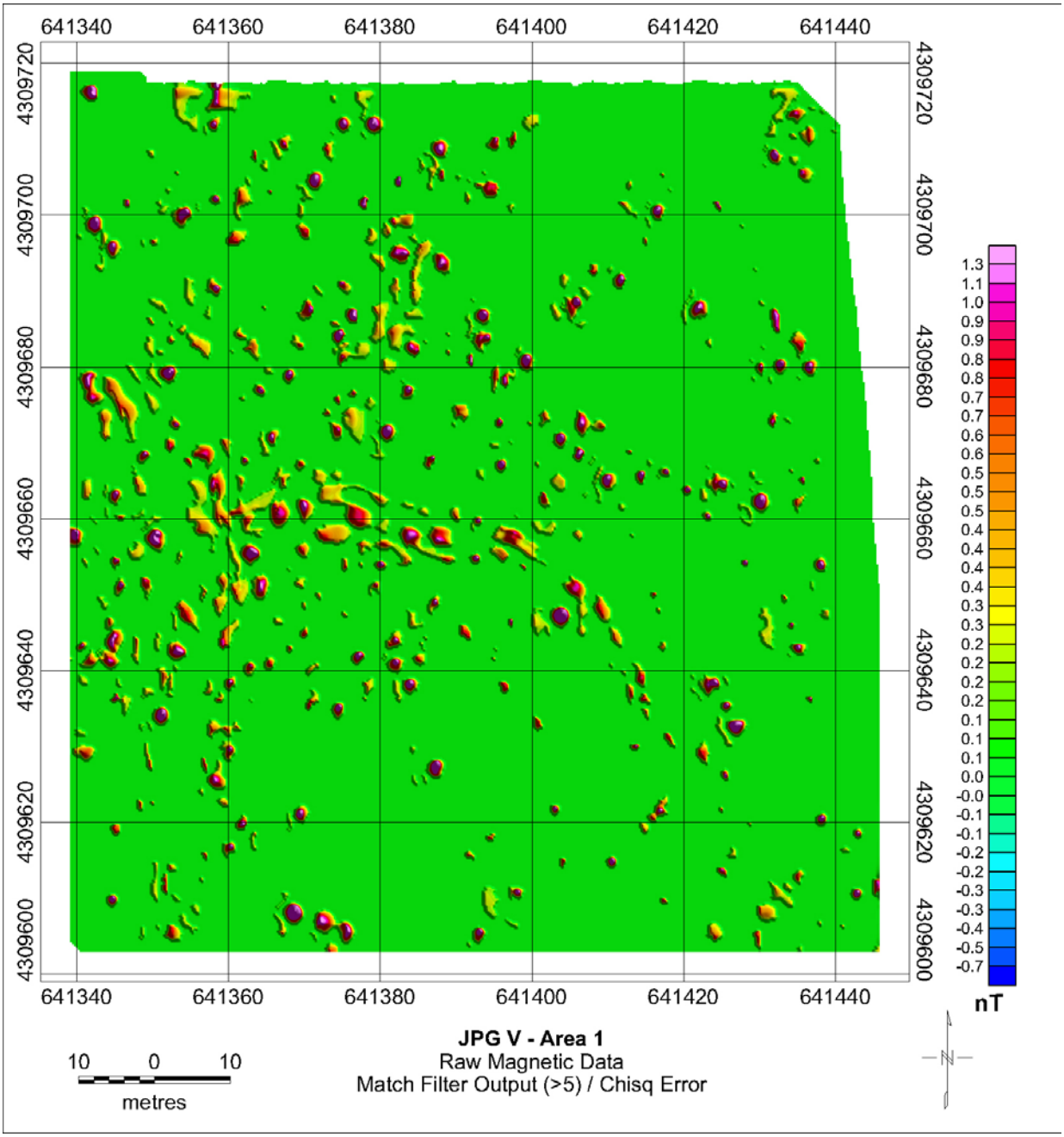

Figure B-11. Color-coded map showing the results of dividing the matched filter output values that are larger than five by the derived model error; Area 1 JPG TD.

Discarding those locations that had a reported depth (depth is one of the fitted parameters) of greater than one meter and an apparent size (apparent size is also one of the fitted parameters) of less than 0.13 m further restricted the data presented in Figure B-12. These data were then used as the final filter output. Potential anomalies were selected using the OASIS Montaj grid peak utility.

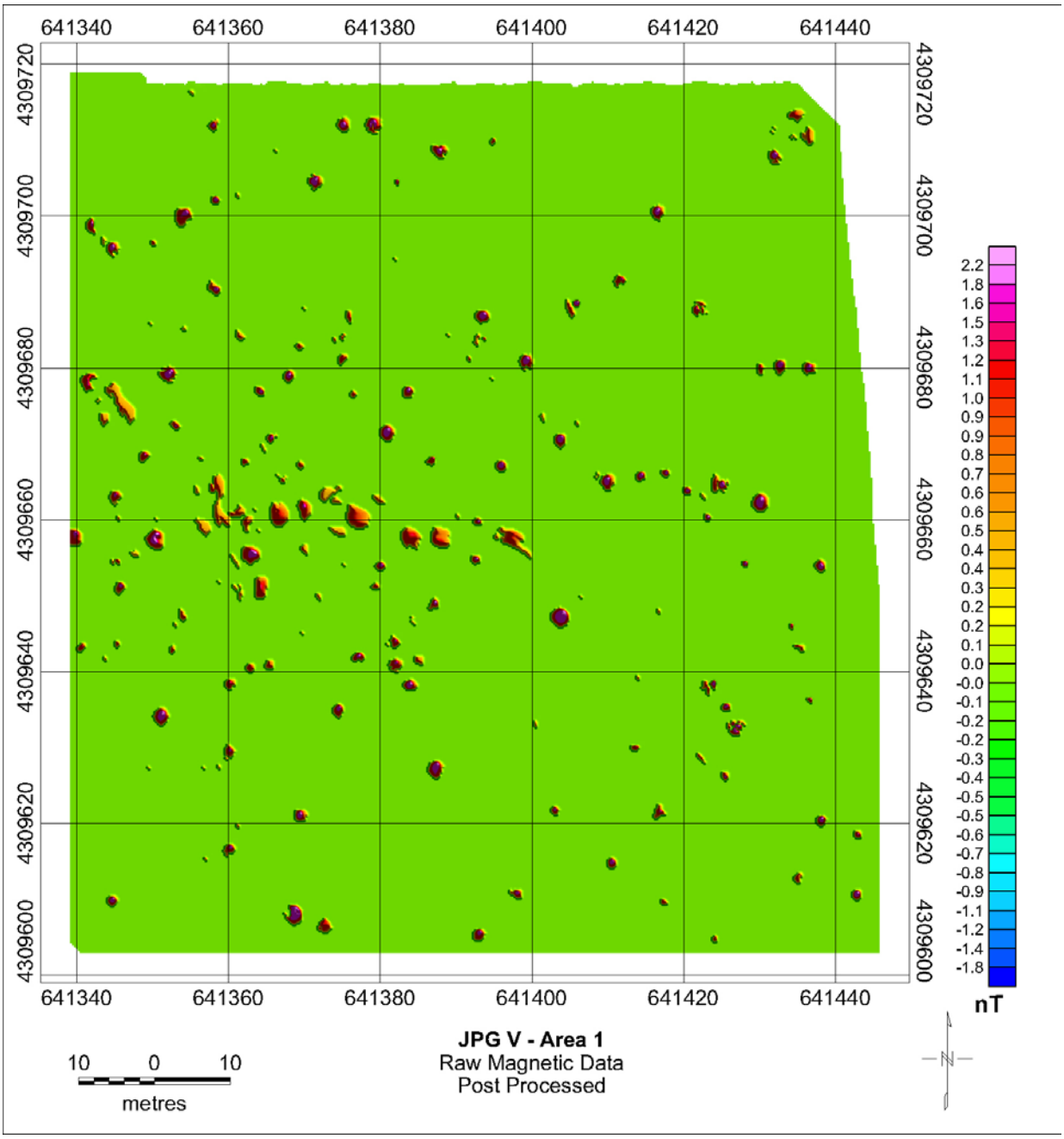

Figure B-12. Color-coded map showing the final post-processed results of the matched filter; Area 1 JPG TD. See text for discussion.

Figure B-13 presents the final post-processed matched filter output grid overlain by the ground truth (+ symbols and text) and the anomalies selected by the grid peak executable (circles; minimum peak value of 0.3). Utilizing the fitted model parameters to improve the filter output (as described above) revealed 11 targets that are not apparent in the unprocessed filter output (compare Figures B-13 and B-14). The additional detected targets included 57mm, 60mm, and 81mm items.

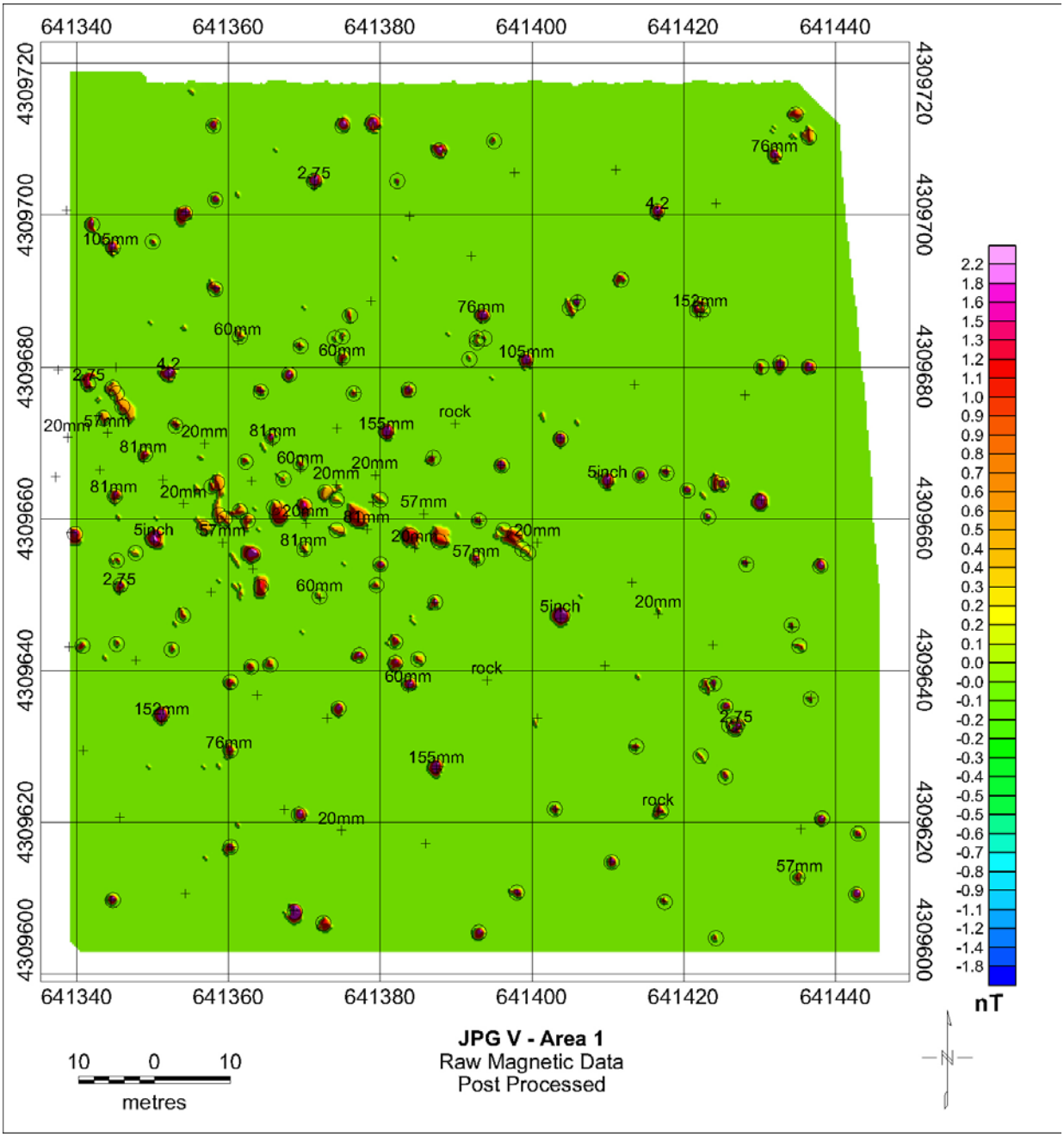

Figure B-13. Color-coded map showing the final post-processed results overlain by the ground truth (+) and anomaly picks (circles); Area 1 JPG TD.

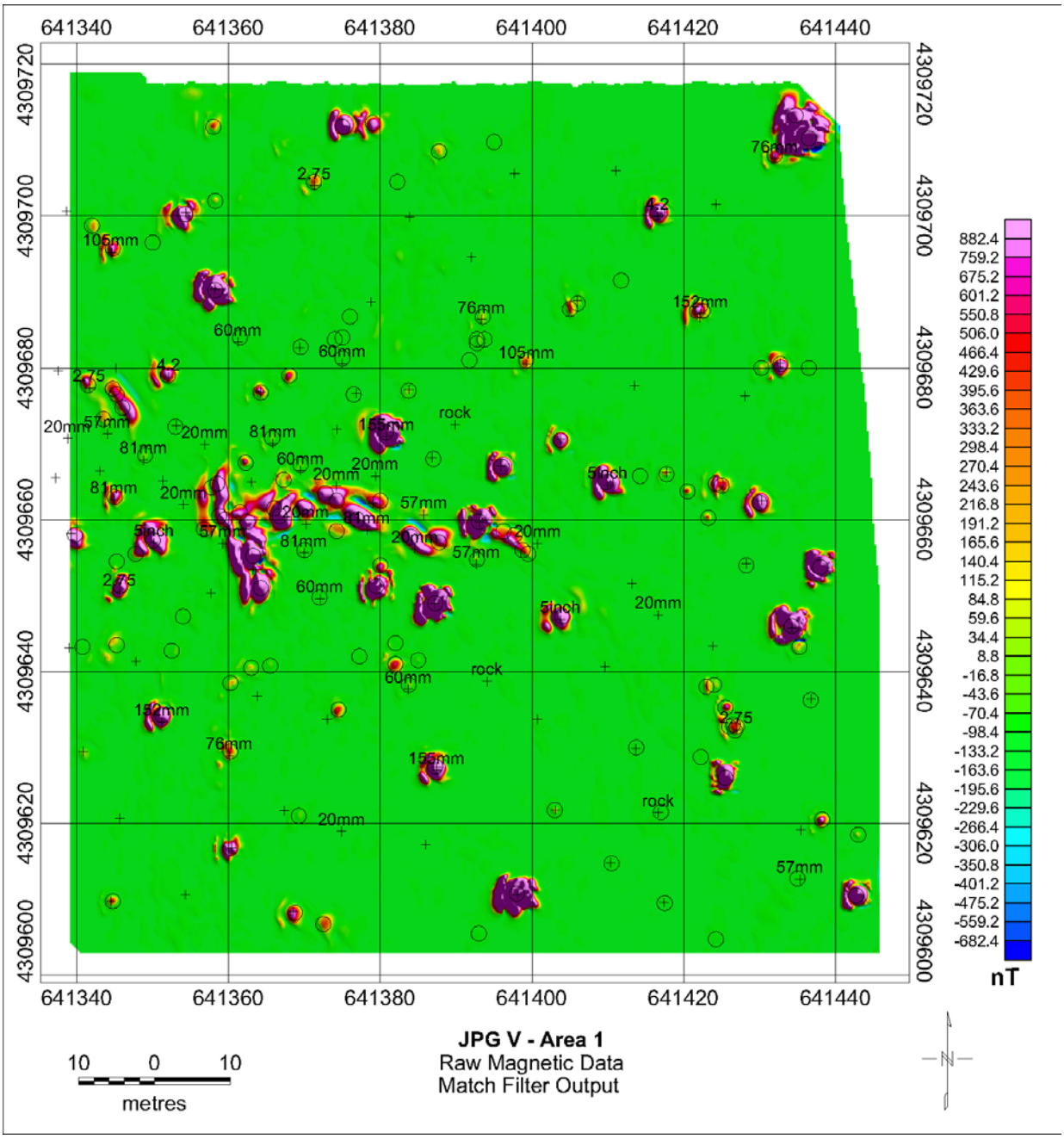

Figure B-14. Color-coded map showing the original matched filter output overlain by the ground truth (+ and text) and anomaly picks (circles); Area 1 JPG TD. Comparing these data with that shown in Figure B-13 indicates that utilizing the model parameters to post process the filter results identified an additional 11 emplaced targets.

The anomalies identified after screening using the IDL prototyped filter are superimposed (using square symbols) on the final processed OASIS Montaj matched filter results in Figure B-15.

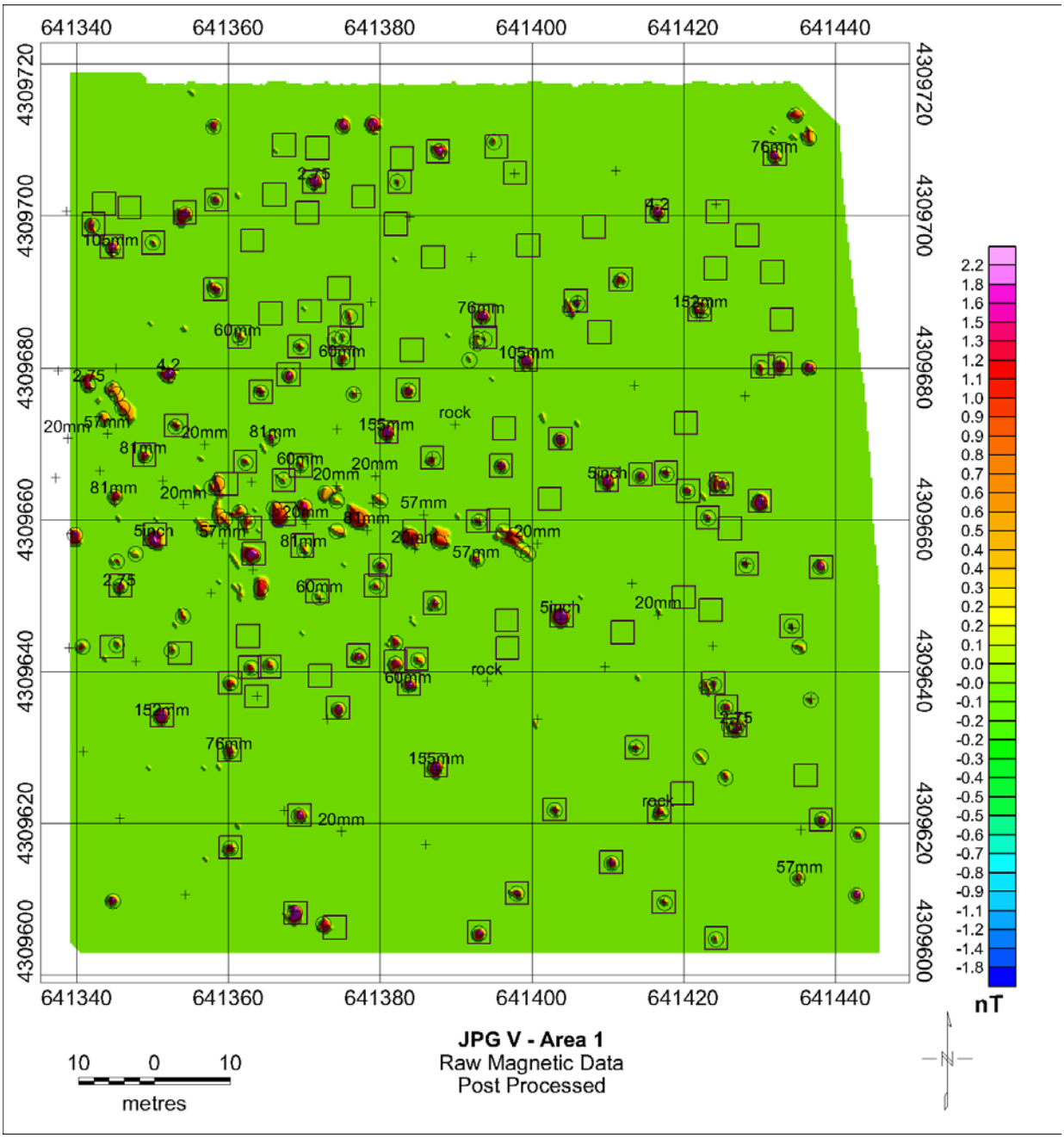

Figure B-15. Color-coded map showing the final post-processed results overlain by the ground truth (+), OASIS Montaj matched filter anomalies (circles), and anomaly picks (after screening) using the IDL matched filter algorithm (squares); Area 1 JPG TD.

In summary, a total of 150 anomalies were identified for Area 1 using the OASIS Montaj embedded matched filter. Table B-4 presents a comparison of the detected versus emplaced UXO items in Area 1.

Table B-4. Detected versus Emplaced UXO items in Area 1, JPG TD

Ordnance Type	Number Identified	Emplaced
20mm	0	10
57mm	2	5
60mm	5	5
76mm	3	3
81mm	4	5
105mm	2	2
152mm	2	2
155mm	2	2
4.2 inch	2	2
5 inch	3	3
2.75 inch	4	4
Total	**29**	**43**

For these data, the detection rate was 67% primarily because, as noted in Table B-4, none of the 20mm items produced peak values above the selected threshold of 0.3. This is not unexpected based on our previous experience with the IDL prototyped matched filter and the almost negligible measured response associated with the 20mm's (Figure B-16). If the 20mm items are excluded, the detection rate increases to 88%. The three missed 57mm items were located near magnetically active regions and probably would not be detected visually (Figure B-16). The missed 81mm item was also located within an active magnetic area and is not readily apparent when the raw magnetic data are inspected visually (Figure B-16).

The percentage of items declared as potential targets by the matched filter algorithm that are not emplaced ordnance items is approximately 80%. This is similar to number of false alarms reported during the previous IDL development.

Figure B-16 presents the raw magnetic data overlain by the identified anomalies from the OASIS Montaj embedded routine (circles) and the ground truth (+ symbol and text). Although some of the matched filter target selections would probably be discarded after visually inspection, we did not do so to preserve this evaluation of the filtering approach.

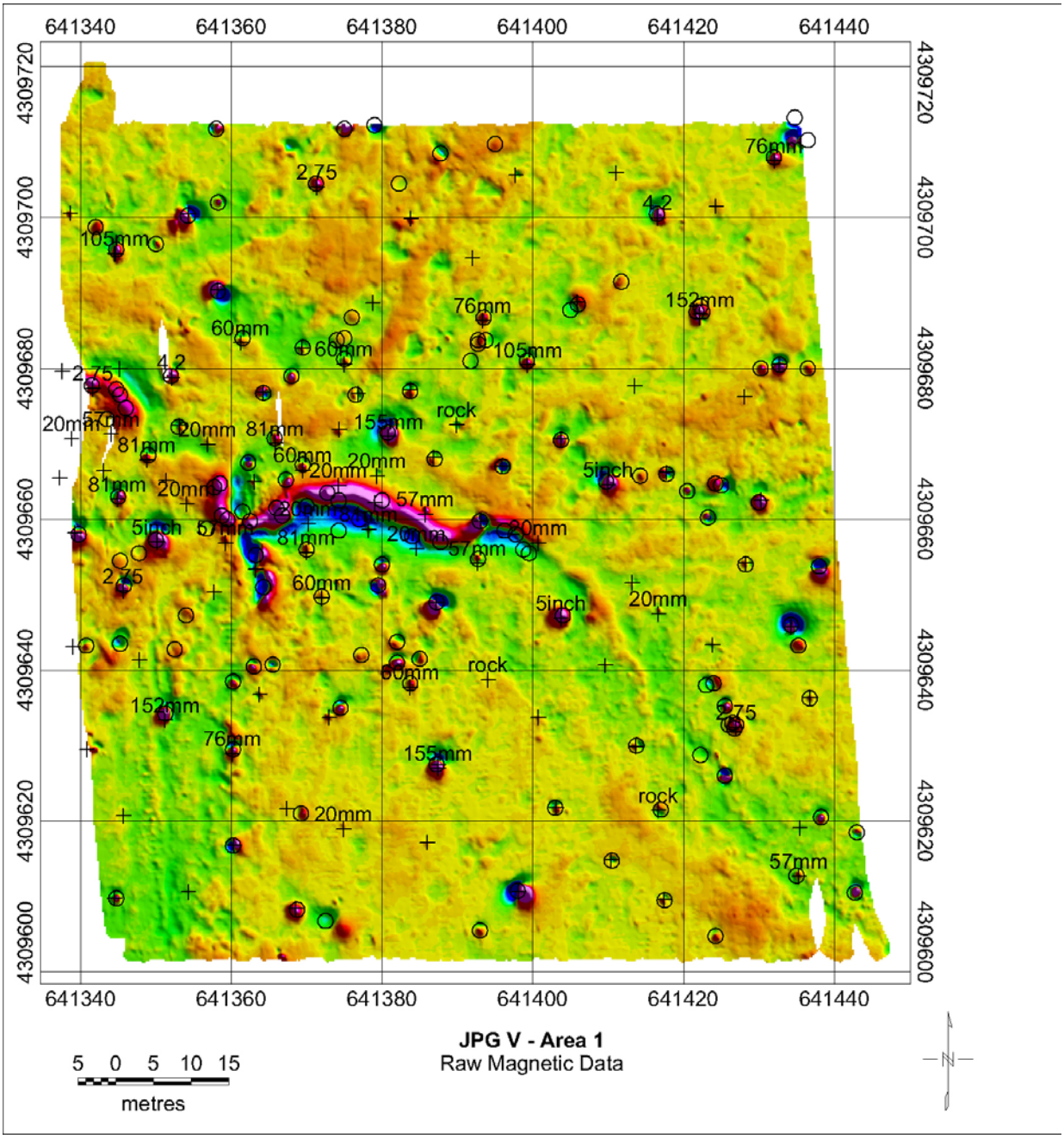

Figure B-16. Color-coded map showing the raw magnetic data overlain by the ground truth (+) and anomalies identified by the OASIS Montaj embedded matched filter routine (circles); Area 1 JPG TD.

ESTCP Program Office

901 North Stuart Street
Suite 303
Arlington, Virginia 22203

(703) 696-2117 (Phone)
(703) 696-2114 (Fax)

e-mail: estcp@estcp.org
www.estcp.org